SAND2023-07340T

Plume-Targeted Cooling Effects for High- and Medium-Density Metals Fabricated by Controlled Atmosphere Plasma Spray

A Thesis Presented

by

Emma Peleg

to

The Graduate School

in Partial Fulfillment of the

Requirements

for the Degree of

Master of Science

in

Materials Science and Engineering

Stony Brook University

August 2023

Stony Brook University

The Graduate School

Emma Peleg

We, the thesis committee for the above candidate for the
Master of Science degree, hereby recommend
acceptance of this thesis.

Sanjay Sampath – Thesis Advisor
Distinguished Professor, Materials Science and Chemical Engineering

Richard Neiser – Second Reader
Adjunct Professor, Materials Science and Chemical Engineering

Jonathan Sokolov – Third Reader
Professor, Materials Science and Chemical Engineering

This thesis is accepted by the Graduate School

Celia Marshik
Interim Dean of the Graduate School

Abstract of the Thesis

Plume-Targeted Cooling Effects for High- and Low-Density Metals in Controlled Atmosphere Plasma Spray

by

Emma Peleg

Master of Science

in

Materials Science and Engineering

Stony Brook University

2023

Thermal spray processes benefit from workpiece cooling to prevent overheating of the substrate, retain metallurgical properties (e.g., temper), and control the thermal component of residual stresses. Cold-gas "plume quenching" is a plume-targeting cooling technique, where an argon jet is directed perpendicularly to the plasma jet and far enough downstream that most particle heating and acceleration is complete. The intent is to redicret the high-temperature plasma gases away from the substrate without impacting particle temperature and velocity. However, there has been little investigation of its effect on molten particles in the plume and the resulting coating properties. This study examines high- and medium-density tantalum and nickel coatings, fabricated with Controlled Atmosphere Plasma Spray with and without the addition of plume quenching on aluminum and titanium substrates. To observe the direct effects of plume quenching on the plume, Differential Flame Thermometry was used to examine substrate temperature and plume spot size. To compare the effect of plume quenching on coating deposition, the deposition efficiency was calculated through coating mass gain, and the coating density, stiffness, adhesion, and residual stresses were measured.

Tantalum and nickel coatings were largely unaffected by plume quenching with respect to deposition efficiencies, coating density, adhesion and stiffness, plume quenching generally reduced residual stress amongst most substrate-coating pairings. These results indicate that a plume quench can be used without affecting the coating properties for high- and medium-density metals while providing the benefits of substrate cooling that increases with higher plume quench gas flow rates.

Table of Contents

List of Figures:

List of Tables:

List of Abbreviations

APS – Air Plasma Spray

CAPS – Controlled Atmosphere Plasma Spray

CTE – Coefficient of thermal expansion

SLPM – standard liters per minute

ICP – In-situ Coating Property

ECP – Ex-situ Coating Property

Acknowledgments

I would like to acknowledge Professor Sanjay Sampath and the members of the Center for Thermal Spray Research at Stony Brook University for their continued guidance and support during both my undergraduate and graduate years. I would like to thank my postdoctoral and staff mentors that have guided me in learning thermal spray and conducting research: Dr. Juliane Ribeiro da Cruz Alves, Dr. Felipe Caliari, and Dr. Eugenio Garcia-Granados. I would also like to acknowledge the students that have worked beside me, offering advice and comradery during long days of spraying and always providing discussion and feedback: Rohan Chandakkar, Dr. Shalaka Shinde, Dr. Edward Gildersleeve, Alvin Kim, and Donald McMahon. Thank you all for your candor and ongoing support.

I would also like to thank Professor Sampath for leading me to my current position with the Thermal Spray Research Laboratory at Sandia National Laboratories, where I have continued my graduate studies. I would like to acknowledge the ongoing mentorship from Dr. Andrew Vackel, who has worked continuously with me to develop this body of work and see it through to the end, while allowing me the freedom to formulate and probe my own scientific questions. I would also like to thank Thomas Holmes, who is the mastermind behind the operation of the Controlled Atmosphere Plasma Spray and has taught me everything I know about the system, fixturing, and machining. A large thanks is also in order to Dr. Michael Kracum, who has provided a critical eye and external perspective to this body of work; much of my work is owing to generosity of his time and insight.

I would also like to thank my current advisory team at the Sandia National Laboratories, consisting of Dr. Michael Kracum, Dr. Brittany Branch, Dr. Chad McCoy, Dr. Corbett Battaile, and Dr. Richard Neiser, who are supporting me in my continuing academic journey. In addition to these Sandians, I thank my previous manager, Joe Fonseca, for his meticulous editing of this document and unfaltering support that has pushed me to continue when I thought I could not.

Lastly I would like to acknowledge the members of my committee, Professor Sanjay Sampath, Dr. Richard Neiser, and Professor Jonathan Sokolov. Thank you for the continuous support, time, effort, and eye-opening conversations that have and will continue fuel my excitement and drive for this field.

This paper describes objective technical results and analysis. Any subjective views or opinions that might be expressed in the paper do not necessarily represent the views of the U.S. Department of Energy or the United States Government.

Sandia National Laboratories is a multimission laboratory managed and operated by National Technology and Engineering Solutions of Sandia, LLC, a wholly owned subsidiary of Honeywell International Inc., for the U.S. Department of Energy's National Nuclear Security Administration under contract DE-NA0003525.

Chapter 1

1.1 Introduction

Thermal spray is a thick-film deposition technique used to deposit ceramic, metallic, and cermet powder feedstocks onto a variety of substrates. With the ability to apply coating thicknesses from micron to millimeters at fast rates, it is used for a wide variety of applications including wear and corrosion resistant coatings, low thermal conductivity coatings for high temperature applications protection, and in quick repairs requiring material reapplication [1].

Plasma spray is a high-temperature process, achieving temperatures between 6000 °C to 15,000 °C in the initial powder heating region [2]. This makes it a suitable process for high-melting point materials, such as ceramics and refractory metals. Refractory metals are characterized by their high temperature performance, as well as good wear and corrosion resistance; a result of a thin oxide layer forming on their surfaces when exposed to ambient environments [3]. These resistive properties are desirable on a macroscopic scale but can be detrimental to the integrity of plasma sprayed coatings because of the unique fabrication method, which causes ambient atmospheric constituents to interact with the individual particle exteriors as they are injected into the spray "plume" at high temperatures. As particles melt and deposit into layers of "splats" that form a coating, the oxidized exteriors reduce the interlamellar adhesion, include brittle oxide stringers, and lose the bulk properties of the initial metallic feedstock [4]. There are few techniques used to mitigate the interaction of atmospheric oxygen and nitrogen, such as inert gas shrouding for APS, or Controlled Atmosphere Plasma Spray (CAPS).

Controlled Atmosphere Plasma Spray, amongst other environment-controlled thermal spray techniques such as Vacuum Plasma Spray (VPS) and Argon Shrouded Plasma Spray (ASPS), is a technique used to maintain coating feedstock purity by reducing or removing reactive atmosphere constituents such as oxygen and nitrogen. CAPS consists of a vacuum chamber capable of high-medium vacuum or inert gas backfill up to positive pressures, fitted with DC plasma spray capabilities.

However, plasma spray is a high temperature process, and runs the risk of workpiece overheating and damage due to temper loss. Heat is imparted onto the substrate both by deposition of molten particles as well as the impingement of hot plasma gases onto the substrate surface. Additionally, the enclosed environment of the CAPS vacuum chamber used in this study restricts

the ability for convective and ambient cooling, while backfilled argon acts as an insulator to trap heat within the system. High workpiece temperatures are a source of thermal stress, a component of residual stress for the coating-substrate pairing [5].

Residual stresses in coatings form due to the differences in temperature gradient within the bulk, particle contraction due to rapid solidification of each droplet during deposition, and are heightened by the mismatching coefficients of thermal expansion between coating and substrate materials. As the coating is formed from the rapid solidification of splats, their thermal contraction is constrained by their adhesion to the underlying substrate, forming tensile stresses within the lamellae [5, 6]. This effect is further enhanced by high-conductivity substrates, and as coatings cool to room temperature and the coating-substrate system contracts. Coating-substrate pairings with residual stresses exceeding the cohesive or adhesive bonding forces of the coatings are susceptible to delamination and cracking, making residual stress control a primary concern for thermal spray fabrication [5].

To reduce workpiece damage and thermally induced stresses, convective cooling techniques such as gas-jet cooling with compressed air, argon, and carbon dioxide have been used to remove absorbed heat, which work by targeting the substrate directly during deposition [6, 7]. Conductive water-cooling plates are also used to remove absorbed heat from a workpiece. However, both convective and conductive cooling techniques target the workpiece itself, which creates issues for complex geometries requiring non-planar deposition (e.g., spinning substrates, robotic motion).

“Plume quenching” is a cooling technique where a perpendicular jet of cool gas is directed into the plume to redirect hot plasma gases without impeding particle motion, thus potentially reducing the need for convective substrate cooling [8, 9]. Unlike other cooling techniques, plume quenching targets the plume itself, removing hot gases before they transfer heat into the substrate. However, little information exists in literature regarding the effect of plume quenching on coating properties. This body of work attempts to further characterize the influence of plume quenching using CAPS. An abbreviated process map examining fundament process effects and coating properties of metals with and without the addition of plume quenching was pursued by investigating:

- The interaction of the plasma gas plume with the plume quench.
- Potential effects on particle temperature and velocity.

- Relative deposition efficiency.
- Coating density and microstructure.
- Coating adhesion.
- Young's modulus.
- Coating residual stresses and their contributing factors.

The results reported here can be used to inform the use of plume quenching as a cooling technique for other materials and thermal spray processes.

1.2 Objectives

The objective of this study is to produce CAPS-fabricated nickel and tantalum coatings with and without the use of plume-targeted cooling to examine the technique's potential for substrate cooling and stress mitigation, while documenting any effects of the plume quenching on the coating properties. Investigating the capabilities of this technique for medium- and high-density metal powders will serve as an useful step in designing non-conventional cooling techniques and predicting any potential effects on the coating properties.

Chapter 2
Background

2.1 Thermal Spray for Coating Fabrication

Coatings are used in a wide variety of applications and range from thin to thick films between the nano- to macroscale. Thin film coatings are typically formed using Chemical and Physical Vapor Deposition (CVD/PVD), sputtering, and electroplating, and produce nano-scale films deposited at very low rates. Thick-film coatings can be applied by techniques such as screen-printing, painting, and thermal spray, and produce macro-scale films often at faster rates. Thermal spray is a technique categorized by its rapid deposition rate and ability to produce viable coatings at low costs and high volumes, making it an efficient technique for a wide variety of industrial applications. It is a way to fabricate high melting point materials that prove challenging with other traditional techniques. Some critical applications use these coatings as supporting technology for wear and corrosion protection, heat conduction and insulation, as well as fast depositing mass gain and repair. These coatings have also been considered for high-porosity catalytic materials, sensors, fusion reactor core materials, and other prime reliant components [10, 11].

As a thick film technique, thermal spray is used to produce coatings by both kinetic and thermal mechanisms. This is done by depositing powder feedstock particles accelerated through a torch, typically carried through a DC or RF plasma arc or combustion-based flame [1]. The combination of heat source in the torch, powder feedstock (metallic, ceramic, or cermet), and carrier gas used to inject the particles into the torch is referred to as the "plume". As molten particles are deposited, they flatten into disks and rapidly solidify, adhering upon impact. These fundamental coating building blocks, solidified discs, are commonly referred to in literature as "splats". Upon the first pass of a thermal spray torch, these splats interact directly with the substrate and form a mechanical interlocking, although it has been shown that metallurgical bonding can also be present on a small scale for some substrate-coating pairs [12]. To achieve a desired coating thickness, multiple passes are made by the torch as splat deposits build and increase in thickness with the application of new layers. The thermal spray process is highly disordered, and external factors such as non-uniform powder feedstock, varied heat distribution, and atmospheric interaction with the plume are all sources of variability. The result of this is microscopically stochastic but macroscopically uniform coatings, with embedded porosity and oxides due to

imperfect layering and in-flight oxidation. Due to their efficiency and versatility, thermal sprayed coatings are continually explored for existing and new applications.

2.2 Plasma Spray Theory and Splat Behavior

Plasma spray uses an arc generated using a high DC or RF current, reaching temperatures capable of ionizing gas, generating plasma, and melting both metals and high melting point ceramics [13]. A typical plasma spray torch will consist of a copper anode and tungsten cathode which form a plasma arc when a high voltage is applied during ignition. Plasma-forming gases (such as argon) flow around the cathode and surrounding anode (labeled in Figure 1) and are transformed into plasma from contact with the high temperatures. A combination of water and air cooling surround the plasma torch, stabilizing and isolating the gas flow such that it extends from the nozzle and forms a plume, as shown in Figure 1.

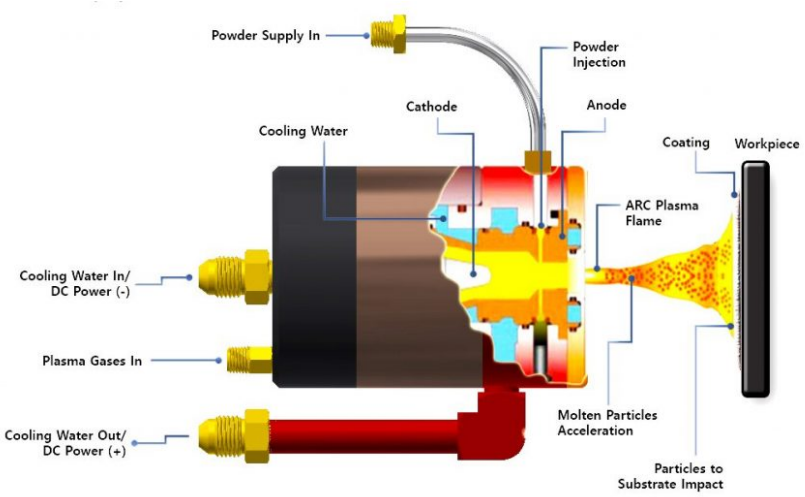

Figure 1. SG-100 plasma spray torch diagram [14].

During deposition, powder feedstocks are injected into the plasma using a carrier gas which merges with the plume either externally or internally as shown above in Figure 1. The combination of carrier and auxiliary gases flowing through the torch accelerate the feedstock particles while simultaneously melting them. As they impinge on the substrate, they layer and form a coating with highly random splat structure and configuration, which establish the properties of the coating bulk.

2.3 Plasma Spray for Metallic Feedstocks

Plasma spray is well suited for depositing both metals and ceramics due to its high temperature capabilities. For high-melting point refractory materials with good wear and corrosion

resistance, plasma spray can be used to fabricate thick-films for automobile, aerospace, and marine applications that would otherwise be challenging to fabricate [5]. The metal feedstocks used for this study are refractory tantalum, and nickel. These two metals are used industrially for a variety of applications and were chosen for this study to compare the behavior of high- and lower-density metals (powder density playing a role in the potential for particle deflection by plume quenching) under plume-targeted cooling (a technique described in section 2.5.2 Plume Targeted Cooling: Plume Quenching). Tantalum coatings have been used to develop sputtering targets, surgical implants, and in the development of first wall coatings in nuclear fusion devices such as tokamak research reactors [15, 16]. Nickel is highly corrosion resistance and can be sprayed onto seawater facing surfaces as well as other corroding chemical environments.

2.3.1 Nickel and Tantalum Powder Feedstocks

Tantalum is a high-density refractory metal (16.6 g/cm^3), with a melting point of 2996 °C. It is known for its good wear and corrosion resistance under corrosive and tough environments, which is attributed to the formation of a thin surface oxide layer when exposed to ambient environment [17]. Air Plasma Sprayed (APS) tantalum forms several oxides, most commonly a stable Ta2O5, although other less stable oxides TaO_x can also form as a result of rapid interaction with atmospheric oxygen [18]. Although oxides provide a protective layering they are also characteristically brittle, and tend to crack in response to stresses induced from thermal expansion and mismatch during deposition [5]. Oxide content is also heightened with the increase in interfaces generated by individual particles, with smaller particle feedstock increasing the total surface area exposed to oxidation. Tantalum also has a Coefficient of Thermal Expansion (CTE) of 6.5 $\frac{\mu m}{m - ^\circ C}$.

Nickel is a medium-density transition metal (8.9 g/cm3), with a melting point of 1455 °C. It is relatively stable in ambient atmosphere and does not oxidize easily. Nickel has a CTE of 13.1 $\frac{\mu m}{m - ^\circ C}$, approximately twice that of tantalum.

Table 1. Material Properties for Nickel and Tantalum [19]

Property	Tantalum	Nickel
Melting Point [°C]	2996	1455

CTE $[\frac{\mu m}{m - ^\circ C}]$	6.5	13.1
Density [g/cm^3]	16.6	8.9
Crystal Structure	Body-Centered Cubic	Face-Centered Cubic

2.4 Controlled Atmosphere Plasma Spray

Controlled Atmosphere Plasma Spray (CAPS) is a process used to generate chemically pure coatings from reactive feedstocks by spraying in an inert, typically argon-backfilled environment, reducing interaction with atmospheric constituents such as oxygen and nitrogen. Each spray run requires pumping down to remove any atmospheric constituents before refilling the chamber with backfilling gas (argon, nitrogen). Coatings fabricated in inert atmospheres exhibit lower levels of oxide stringers and impurities and thus have different bulk properties from those fabricated with APS [4, 20]. While a thin layer of oxide is usually beneficial as a protective coating for wear and corrosion resistance, particularly in refractory metals, the oxide formation occurring on the individual splat-to-splat scale decreases the bulk purity, creating metal/metal-oxide interfaces and influencing the overall coating properties by embrittlement and weakened bonding.

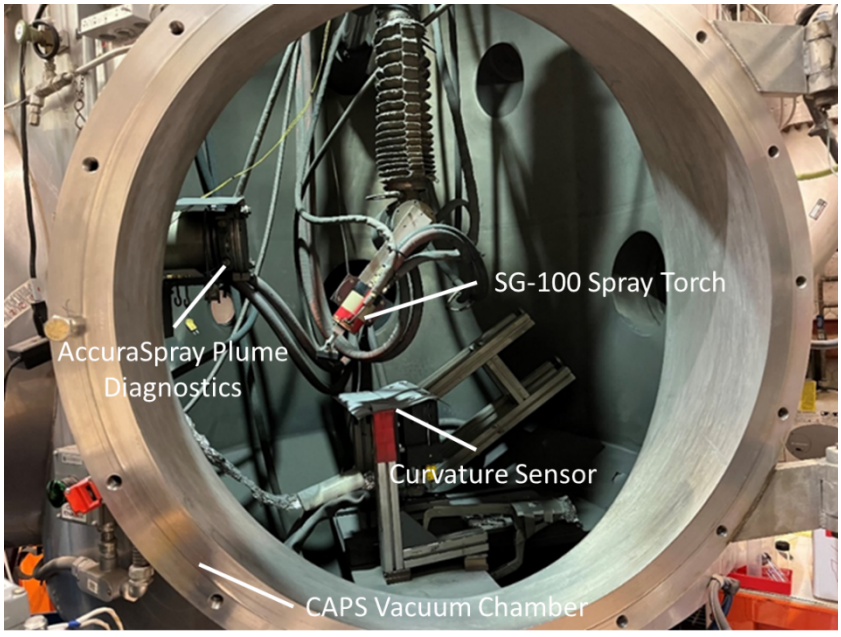

Figure 2. The CAPS chamber at the Thermal Spray Research Lab, configured for In-Situ Curvature Measurements

However, while CAPS prevents reactions with atmospheric constituents, it does not mitigate any of the temperature effects of the plasma arc during processing. Inert gas traps heat within the spray chamber and generally creates higher temperatures than its air-sprayed counterpart, where the surrounding environment provides additional convective cooling. For this reason, cooling techniques are an important tool for CAPS processing.

2.5 Plasma Spray Modifications: Substrate versus Plume Targeted Cooling

Plasma spray can be modified to suit different industrial needs. For plasma spray, two high priority processing conditions are workpiece temperature and atmospheric interactions with reactive constituents (which is resolved by the CAPS process described in section 2.4 Controlled Atmosphere Plasma Spray). There are a variety of established cooling techniques that use conduction or convection to remove absorbed heat from the substrate, such as water-cooling plates and workpiece-targeted gas jets, respectively.

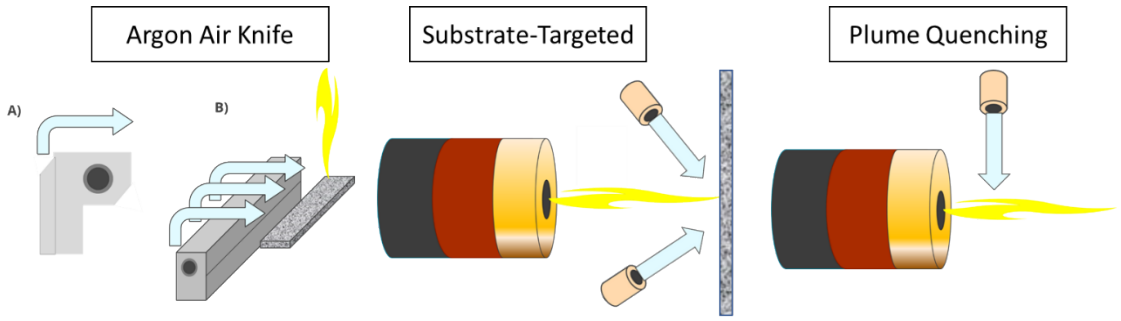

Figure 3. Gas jet cooling techniques, argon air knife, substrate targeting cooling, and plume quenching.

2.5.1 Substrate-Targeted Convective and Conductive Cooling

Standard cooling typically consists of convective and conductive cooling, in the form of gas jets, water-cooling plates, lateral gas air knifes, and other substrate-targeted heat removal techniques. Time off-part is also used to supplement the existing cooling mechanisms by allowing more time for the heat to be removed. These techniques aim to remove heat absorbed by the substrate from both the molten particles and the hot carrier gases as they impinge and interact with the substrate.

While these techniques are effective at removing already absorbed heat from the workpiece, some cases may benefit from reducing the overall heat absorbed, as well as the complexity of designing substrate-specific cooling (particularly in the cases of temperature

sensitive workpieces, manufacturing of complex geometries, or reducing time off the part as a means of increasing efficiency). For the instances when existing substrate-targeted cooling methods are not adequate, additional time off-part would be needed, decreasing the efficiency of the spray process and potentially wasting powder feedstock, gas, and production time.

2.5.2 Plume Targeted Cooling: Plume Quenching

Plume quenching is a cooling technique which, unlike other conventional cooling methods, targets the plume itself and the hot gases within it. The impact of "auxiliary air-cleaning nozzles" and "transverse air curtain" was previously examined by Kiilakoski et. al [8] for its use in High-Velocity Oxy-Fuel Spray (HVOF). For this body of work, "air curtain" will be referred to as plume quenching and describes a technique that uses inert gases such as argon to redirect the hot gases within a spray plume without impeding the particle motion. The plume quench bisects the plume perpendicularly and does not interact with the substrate directly, such as shown in Figure 3.

For the use in HVOF-sprayed Cr_2O_3, plume quenching was shown to reduce surface roughness, while maintaining the hardness of the coating and increasing homogeneity. Additionally, the interlamellar cohesion of the coatings was examined using cavitation erosion experiments, where well-bonded and highly cohesive coatings have a stronger cavitation resistance. It was found that at moderate plume quench gas pressures, the cavitation resistance was increased significantly when compared to the control, non-quenched condition. This result was thought to be due to a reduction of fine particles within the splat boundaries, presumably carried out of the plume by the plume quench. At higher plume quenching gas pressures, cohesion began to reduce which is thought to be the result of the plume quench both cooling and reducing the velocities of the particles. In a study by Kramer conducted at Sandia National Laboratories, a similar bisecting stream of argon referred to as a "flame quench" was also cited as a method of reducing "heat flux" into the substrate [9]. It was reported to divert low-density alumina feedstock, but have no effect on high density tantalum.

The general benefits of plume quenching have been shown for HVOF and Suspension-HVOF (SHVOF), at moderate plume quenching gas pressures. Any level of plume quenching gas pressure was shown to reduce the roughness and defect quantity in the coatings, which is thought to be a result of reduced heat load on the samples in addition to minimization of fine particle inclusions. This study also explored air cooling nozzles, which found that overly high air-cooling

gas pressures were shown to create turbulence at the workpiece surface, decreasing hardness, and increasing surface roughness and consequent cohesion.

The plume quench technology is fixed to the spray torch itself rather than the workpiece or external fixturing, making it a workpiece-agnostic technique that becomes part of the torch itself. By targeting the plume exclusively, hot gases are redirected away from the substrate and the need for cooling applied directly to the substrate is reduced or eliminated. The accessibility of plume quenching makes it a good cooling option for complex workpieces requiring a moderate reduction in substrate temperature.

2.6 Effect of Substrate Temperature on Thermal Spray Coatings

Substrate temperature has effects on the interfacial adhesion mechanisms as particles first impinge onto a substrate, the workpiece temper, and coating properties such as residual stress [21, 22]. In order to control the high temperatures generated by thermal spray, convective cooling is often implemented to prevent workpiece overheating during deposition, using an inert or non-reactive gas to remove heat from the part. Cooling is typically directed towards the workpiece itself, removing heat from the substrate during deposition without interacting with the plume or particles within it (such as gas jets or water cooling backplates).

2.6.1 Effect of Substrate Temperature on Thermally Induced Residual Stress

The temperature differences between substrate and molten particles, rapid solidification and quenching during deposition, and mismatching Coefficient's of Thermal Expansion (CTE) between materials contribute to a residual stress state for the coating. Depending on the substrate-coating materials and temperatures, the final state of residual stress varies between compressive and tensile, depicted in Figure 4. Under the assumption of perfect interfacial bonding and elastic cooling, the final stress state of the coating and substrate system can be described by the sum of stresses generated by particle quenching (deposition stress) and CTE mismatch (thermal stress). The dominating contributor to residual stress can vary based on coating-substrate pairing, processing, and temperature (for pairs with small CTE difference the deposition/quenching stress may be the dominant contribution to residual stress). Figure 4 shows how CTE mismatch and substrate temperature drive the final stress state of the coating, where the degree of substrate expansion is determined by its temperature, with higher temperatures driving higher thermal stresses. For substrates with larger CTE's than their coatings ($-\Delta\alpha$), thermal stress becomes

compressive, with the opposite occurring for substrates with smaller CTE's (+Δα) where thermal stress becomes tensile. Cooling for substrate temperature control can be used to adjust the extent of thermal expansion and resulting thermal stress.

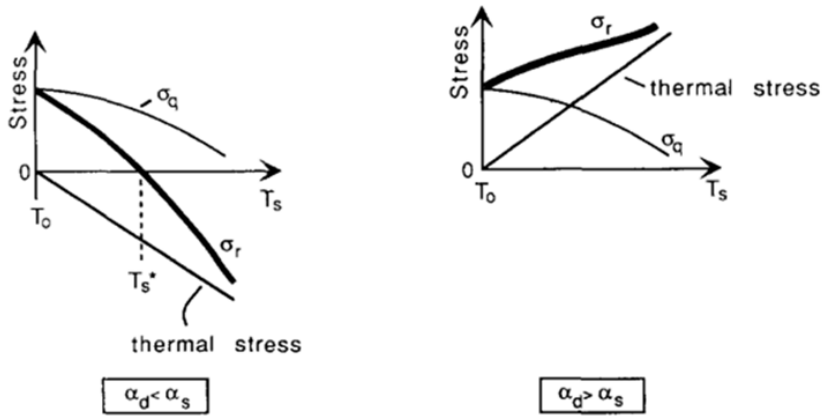

$$\sigma_r(T_0) = \{\sigma_q(T_s)/E_d(T_s) + (\alpha_d - \alpha_s)(T_s - T_0)\}E_d(T_0)$$

Figure 4. Diagram depicting various possibilities for final residual states, where σ_q is quenching stress, σ_r is the residual stress, T_0 is ambient temperature, T_s is substrate temperature, E_d is the Young's modulus of the coating at the temperature T_x, and α_s and α_d are the CTE's of substrate and coating, respectively.

Residual stresses can be relieved or distributed through a variety of mechanisms, such as delamination, edge relaxation, interface sliding, and microcracking. For brittle, ceramic, or oxidized coatings, microcracking can occur when residual stresses overcome the cohesive or adhesion bonding forces of the coating lamellae. For metallic and non-oxidized coatings, such as those fabricated in CAPS, microcracking presence is significantly reduced due to the ductile nature of the bulk material [4].

2.7 Substrate Temperature Management using the Plume Quenching Technique

Although thermal management is not new to thermal spray, the technique proposed in this study targets the hot gases in the plume in an attempt to redirect them from the substrate and prevent heat from being absorbed, rather than the typical convective cooling that is used to removed the already absorbed heat from the workpiece. The substrate temperature during thermal spray deposition has been shown to affect the thermal component of residual stress in coatings, which is investigated in this study with the addition of plume quenching at different flow rates and

for different coating and substrate pairings. The benefit of plume quenching also extends to complex workpiece geometries, which may require complex conventional cooling if targeted at the workpiece, but can be avoided by using a “substrate-agnostic” plume quenching jet which is fixed to the torch instead.

Chapter 3
Experimental Methods

3.1 Spray Processing

3.1.1 Controlled Atmosphere Plasma Spray

The Thermal Spray Research Laboratory (TSRL) at Sandia National Laboratories features a CAPS spray system, featuring an SG-100 plasma spray torch within a sealed chamber, operated in an inert atmosphere backfill such as argon in order to reduce the inclusion of oxides and nitrides formed as particles rapidly react within the plume (described further in section 2.4 Controlled Atmosphere Plasma Spray) [20]. The CAPS system at Sandia National Laboratories is setup in a vacuum chamber that can be backfilled to 5 atmospheres of positive pressure or kept in vacuum during spraying. This allows for the chemical preservation of material purity, especially for materials with a high affinity for oxidation.

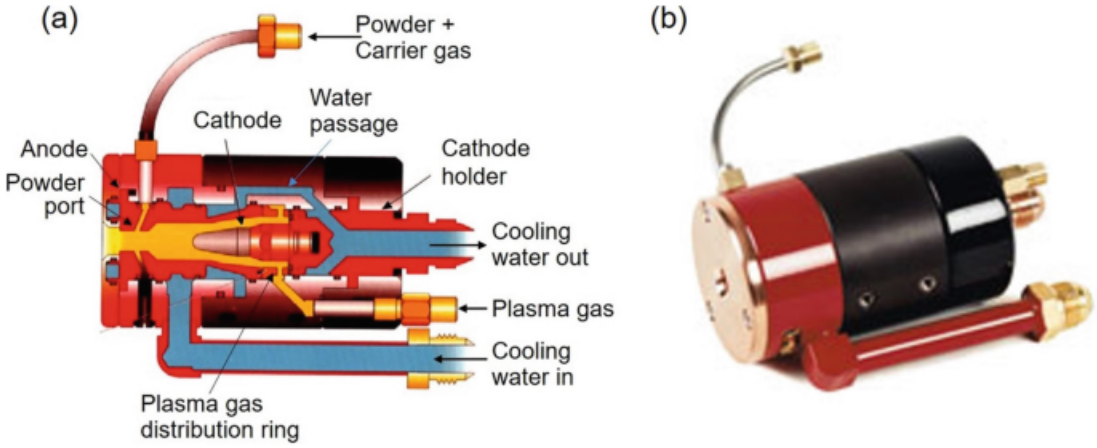

Figure 5. SG-100 Plasma Spray Torch a) internal diagram, b) external view [23]

The coatings fabricated in this study were tantalum and nickel on aluminum and titanium substrates. The plasma spray process parameters used for this study were based on those used at TSRL. All nickel coatings were fabricated using the “Break-In” condition, which uses more argon and a higher current than “SN-Low” but does not include helium in the plume. The tantalum coatings were sprayed using the “SN-Low” condition. Both conditions are based on conditions

established in a paper written by Sampath and Neiser, and adopted by TSRL and described in Table *2* [24].

Table 2. Spray conditions used in CAPS processing

Spray Conditions	SN-Low	Break-In
Torch	SG-100 (Internal Injection)	
Nozzle	730	
Cathode	720	
Ring	112	
Argon Backfill Pressure (Torr)	640	
Spray Distance	100 mm	
Argon (slpm)	50	
Helium (slpm)	12	0
Current (A)	540	500
Plume Quench Flow (slpm)	0/50/100	
Argon Powder Gas (slpm)	3	
Powder RPM	1	
Spindle Fixture RPM	100 CW	
Preheat Passes	2	

3.1.2 Differential Flame Thermometry

A Differential Flame Thermometer (DFT) was used to study the effect the plume quench has on substrate surface heating when directed into the plasma plume (absent of powder feed) as well as the plume quench's ability to directly cool the substrate surface after being heated. The DFT consists of a sandwich of 8-PCF Cerablanket ceramic fiber insulation held between two Inconel plates (painted with high emissivity paint) that are instrumented with type K thermocouples for temperature measurements [25]. A FLIR A6700 MWIR InfraRed (IR) camera was also used to observe the temperature profile of the front Inconel plate during testing in addition to Inconel plates thermocouple measurements.

A series of tests were conducted where the plasma torch was moved to face the center of the DFT and held in place for 5 minutes (or until the front plate temperature exceeded ~850°C). After 5 minutes the torch was immediately extinguished while temperature measurement continued as the DFT cooled. Experiments were run at the two torch conditions found in Table 2 with and without the plume quench on during heating and cooling. Plume quench flow rates studied were 50 or 100 slpm of argon. The DFT was allowed to cool below 40°C after each test prior to beginning the next test.

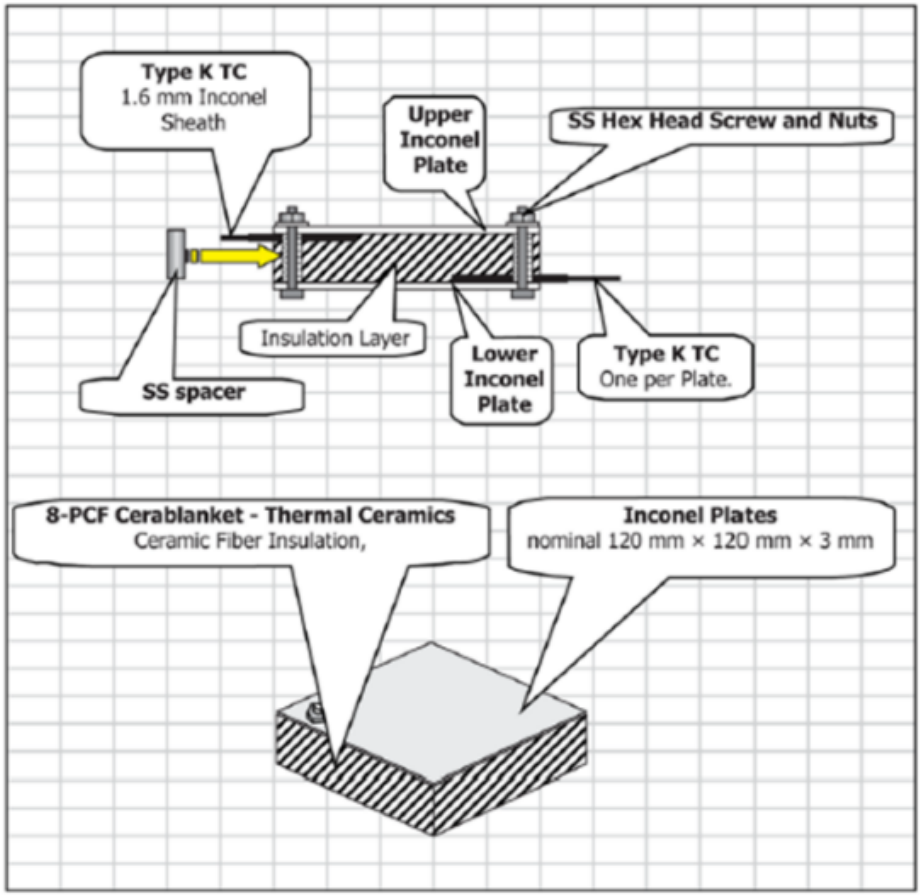

Figure 6. Differential Flame Thermometry (DFT) schematic [25]

3.1.3 Plume Characterization

Particle temperature and velocity were measured using an Accuraspray system (spray diagnostic tool developed by Tecnar Spray Sensors) within the CAPS chamber under argon atmosphere at varying spray distances to observe particle velocity and temperature. Measurements were recorded for tantalum using the SN-Low condition described in Table 2, with plume quenching at 0, 50, and 100 slpm for 60 seconds. Nickel was attempted but not recorded due to experimental difficulties.

3.2 Coating Fabrication

3.2.1 Feedstock

Nickel and tantalum powder feedstocks were used to spray all samples. The feedstock information is show in Table 3. Particle size analysis and chemical analysis were performed on both feedstocks.

Table 3. Nickel and tantalum powder feedstocks.

Powder	Nickel	Tantalum
Manufacturer/Name	Praxair Ni-914-3	H.C. Starck 150.074
Reported Particle Size [μm]	+16/-45	+15/-45

3.2.1.1 Particle size and chemical analysis

Particle Size Analysis (PSA) was performed using a Beckman Coulter LS 13 320 XR Particle Size Analyzer, which uses Polarization Intensity Differential Scattering (PIDS) and laser diffraction to detect particles. This technique allows for the measurement of submicron particles as small as 10 nm [26].

LECO Interstitial Chemical Analysis was performed to detect oxygen and nitrogen content in powder feedstock and CAPS fabricated samples to verify the chemistry. This analysis uses free-standing coatings of samples fabricated with CAPS versus air spray.

3.2.2 Sample Matrix

Samples were fabricated based on the matrix shown in Table 4. All samples were fabricated using CAPS under argon backfill in slight positive pressure of 640 Torr (ambient pressure in Albuquerque, New Mexico; at 625 Torr is lower than standard due to high altitude). The plume quenching "on" condition refers to plume quenching at 50 slpm, with the addition of 100 slpm samples for the residual stress study described in section *3.4.3 Residual Stress Measurements*

(*titanium beams were fabricated for analysis of coating chemistry but were not used further in the study).

Table 4. Sample Fabrication Matrix

	Powder	Substrate	Gas Masking Condition	Spray Condition
Adhesion Buttons & Beams	HC Starck Tantalum	Aluminum	Plume Quench Off/On	SN Low
		Titanium*	Plume Quench Off/On	
	Praxair Nickel	Aluminum	Plume Quench Off/On	Break-In Condition
		Titanium*	Plume Quench Off/On	

Figure 7 shows the two sample geometries fabricated for this study. The geometry in Figure 7-A shows an adhesion "button", which was used to generate "buttons" for the Tensile Adhesion Test (ASTM C633) and to compare coating deposition efficiency, mass, volume, and density with and without plume quenching. Figure 7-B shows a bilayer thermal cycling beam, used to measure coating modulus through thermally induced curvature (described in section 3.4.2 *Bilayer Thermal Cycling*), and for in-situ residual stress measurement (described in section 3.4.3 *Residual Stress Measurements*).

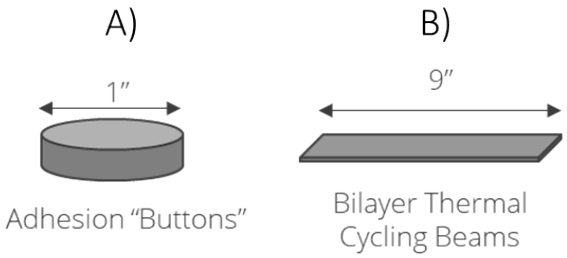

Figure 7. Sample geometries, A) adhesion "buttons", and B) bilayer thermal cycling beams

Prior to spraying, samples were cleaned and prepared by washing and wiping down with acetone followed by isopropyl alcohol to remove and residual grease grit. Bilayer thermal cycling beams were roughened with 600 grit paper before they were cleaned; buttons were kept as machined.

3.2.3 Fixturing

The CAPS system uses a rotating spindle in combination with lateral torch movement to deposit coatings. The CAPS spindle can be fixtured to carry different substrates, such as the buttons and beams shown in Figure 7.

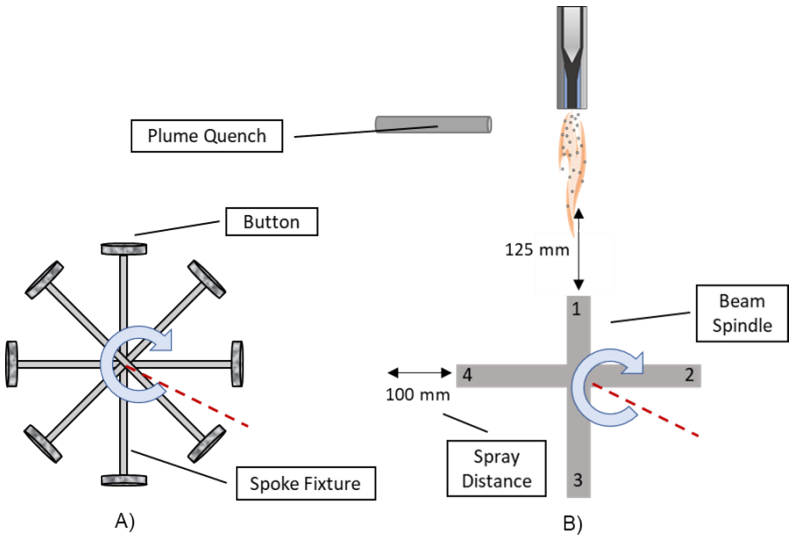

Figure 8. A) Spoke and hub fixture, and B) beam fixture.

Figure 8 shows the two fixturing orientations from a head-on view of the spindle (the red line indicating the axis of torch movement and the arrow indicating spindle rotation) for button and beam fabrication. Figure 8-A is the "spoke and hub" fixture, which carries eight button samples. Four "spoke and hubs" were mounted onto the spindle for each coating feedstock, and spray conditions were changed for each by isolating the torch path. Figure 8-B is used to fabricate beams and labeled 1-4 to indicate the mounting positions of each relative to the spindle's spinning axis. Each fixture contains four beams, one of which is mounted at a slightly lower height to increase spray distance (location 1). Like the "spoke and hub" fixture, the beams are rotated under the spray torch along the indicated axis to deposit along their length.

3.3 Coating Diagnostics

3.3.1 Mass, Volume, Density Measurements

Sample mass was measured using a precision balance scale, and thickness using a ball micrometer. Once prepared and cleaned, sample mass and thickness were taken before being

loaded into the spray fixturing. Once the coated samples were cooled and removed from fixturing, mass and average thickness were remeasured and the difference calculated.

Mass gain was recorded as the different between initial and final buttons. Substrate and coating thickness were measured in 5 locations along the button surface and averaged. The mass gain and calculated coating thickness were used to calculate a volumetric coating density.

Equation 1. Coating Volume for Buttons

$$\pi(\frac{d}{2})^2 \times t_{coating}$$

Mass, volume, and coating density were calculated for all buttons sprayed for repeatability and consistency measurements.

3.3.2 Image Analysis

Image analysis was performed using an in-house program developed at the Thermal Spray Research Laboratory (TSRL), which uses the multi-Otsu method to threshold and distinguish pores and cracks in a coating and calculate the overall porosity [27]. Images were taken from sample cross sections using SEM in Secondary Electron Detection (SED) mode. Each reported porosity was taken as an average of 10 images from the same sample at 500x magnification and reported with error.

3.3.3 Chemical Analysis

As described in Section 3.2.1.1 Particle size and chemical analysis this technique was used to measure oxygen and nitrogen contents in freestanding coating samples for CAPS and Air Plasma Sprayed (APS) materials to verify the importance of CAPS in coating chemistry preservation. Free standing coatings were made by spraying thick deposits (~400 μm) and grinding off the substrate material.

3.4 Coating Properties

3.4.1 Tensile Adhesion Test (ASTM C633)

Tensile adhesion testing was performed following the ASTM C633 standard [28]. The test uses either coated slugs or buttons which are glued to another pulling component to pull apart a coating from its substrate, measuring the interfacial bond strength. For this study, coatings were

sprayed onto buttons glued between two aluminum pulling slugs, and pulled at a constant rate of 13 µm/s; setup is shown in Figure 9.

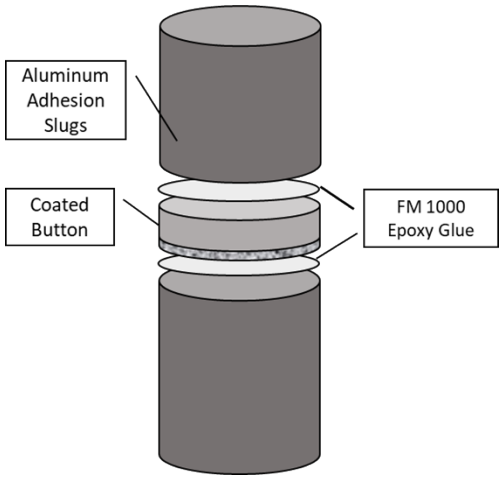

Figure 9. ASTM C633 configuration for buttons

Displacement and force are tracked during the pull and the maximum force at the point of fracture is taken as the peak of the displacement curve. Identically manufactured samples should have relative repeatability and alignment as shown for the samples in Figure 10, indicating consistency in fabrication and test accuracy.

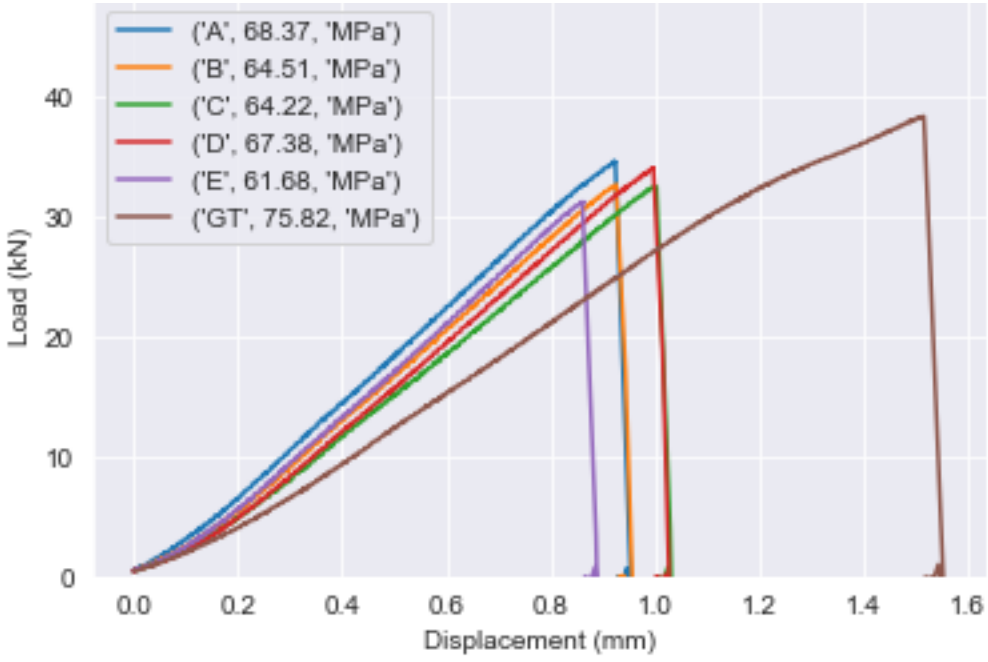

Figure 10. Force vs. displacement curves for a set of 5 samples and one glue test.

Actual adhesion strength at the coating-substrate interface is only measured when the failure occurs solely at that interface. However, multiple modes of failure can occur as shown in Figure 11. Figure 11-A represents a clean failure at the coating-substrate interface, which can be taken at the true adhesion strength of the coating. Figure 11-B depicts failure within the glue portion of the adhesion setup, and while it does not give a concise adhesive strength, the peak strength recorded can be interpreted as a lower boundary threshold for the actual adhesive strength of the coating. Figure 11-C depicts a mixed failure that travels within the coating to some extent; due to the complexity of mixed mode failure this result cannot be interpreted.

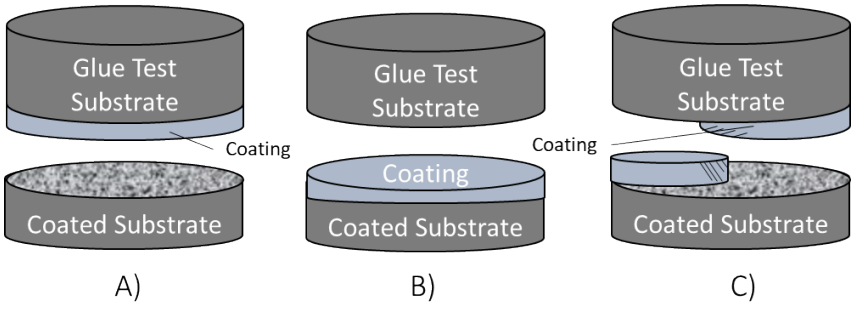

Figure 11. Modes of failure for the ASTM C633 adhesion test

Construction of the adhesion test uses two aluminum slugs that screw into the Instron Universal Testing machine. The surfaces in contact with the glue and sample are grit blasted at 40 psi, and then ultrasonically cleaned in acetone and isopropyl alcohol. The slugs are then sandwiched on either side of the sample using FM-1000 epoxy cutouts and held in place with 100-gram weights and torque at 2 Nm. The fixture carrying the samples is cured at 300 °C for three hours where the FM-1000 epoxy melts, cures, and resolidifies with cooling. The couplings are wrapped with 2” Kapton tape to prevent glue overhang.

Figure 12. Slug and sample fixture for furnace curing

The curing fixture is angled 60° from normal to ensure that the glue sufficiently permeated the top surface while avoiding air bubbles, shown in Figure 12. Samples are also placed within the fixture with the coating facing upwards to facilitate good permeation into the textured top layer of the coating. Once curing is complete and samples are cooled, they are loaded into the Instron Universal Testing machine with the coating facing downwards and pulled until failure.

3.4.2 Bilayer Thermal Cycling

Due to the addition of porosity, microcracking, multiple interfaces, and residual stresses within the coating, the modulus of a thermal coating is much lower [29]. To measure the coating modulus, thermal cycling is a technique that relates the mismatching values for Coefficients of Thermal Expansion (CTE) for a coating and substrate with their respective moduli, and temperature change, shown in Equation 2.

Equation 2. Relationship between curvature change (Δ), mismatching CTE (Δα), temperature change (ΔT), and the modulus for coating and substrate (E'_c and E'_s indicating in-plane modulus (E/(1-ν)) . [30]

$$\frac{\Delta K}{\Delta T} = \Delta\alpha \frac{6E'_s E'_c ht(h+t)}{E'^2_s h^4 + E'^2_c t^4 + 2E'_s E'_c ht(2h^2 + 3ht + 2t^2)}$$

The Ex-Situ Coating Properties (ECP) sensor (developed by ReliaCoat Technologies) shown in Figure 13 holds a sprayed bilayer cycling beam (shown in Figure 7-B) fixed in place on opposite ends, which allows the beam to expand as it is heated to 300 °C. The beam is cycled three times while the temperature and displacement are measured, and then analyzed inversely to extract the stress strain behavior informing the coating modulus.

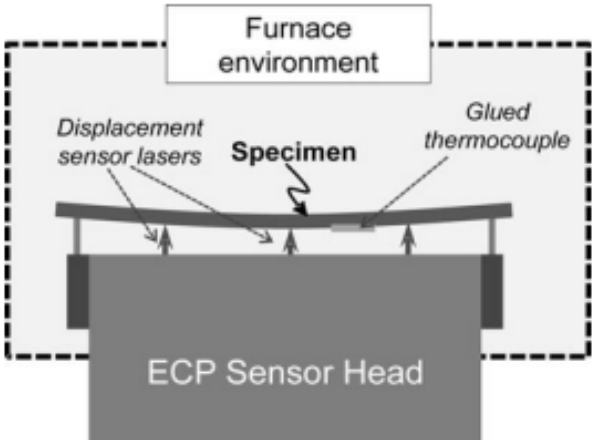

Figure 13. Ex-Situ Coating Properties (ECP) sensor developed by ReliaCoat Technologies [31]

The accuracy of this technique is dependent on knowing the CTE of both the coating and substrate, which for typical APS metallic coatings is variable due to the inclusion of oxides, changing the value itself. Variability in APS metal coatings make it difficult to correct or predict the new CTE value accurately. CAPS produces metallic coatings with negligible oxidation which maintains the CTE and makes them candidates for ECP analysis [4, 32].

ECP analysis was performed for two sets of tantalum coatings sprayed on aluminum beams, with and without plume quenching at 50 slpm. Each set consisted of four total beams, one at an increased standoff as shown in Figure 8-B. The temperature and curvature data collected for all eight samples was used with the values in Table 5 to calculate the coating modulus using Equation 2.

Table 5. Properties used for ECP calculation for Tantalum on Aluminum

Aluminum 6061	
E_s	$68.9 \times 10^9 Pa$

ν	0.33
α	$23.6 \times 10^{-6}/℃$
Tantalum	
α	$6.69 \times 10^{-6}/℃$

3.4.3 Residual Stress Measurements

Like the process detailed in section 3.4.2 Bilayer Thermal Cycling, residual stress measurements in this study relate beam curvature due to CTE mismatch, temperature, and substrate/coating properties to find residual stress. The relationship between residual stress and curvature was first established for thin films by Stoney and adapted for thermal spray films shown in Equation 3 [33].

Equation 3. Stoney Equation

$$\sigma_{Res} = \frac{E'_{sub} t^2_{sub} \Delta K}{6 \times t_{coating}}$$

Residual stress can be broken down into thermally induced stress due to CTE mismatch, and deposition/quenching stress due to the rapid solidification and shrinking of individual particles during deposition. The component breakdown is shown in Figure 4, illustrating the impact of CTE difference and thermal stress on the final residual stress state. Substrates and coatings with large CTE mismatch will drive the final stress state of the coating; compressive when negative, and tensile when positive.

The In-Situ Curvature Properties sensor (ICP) developed by ReliaCoat Technologies measures curvature using laser displacement and backside substrate temperature to record real-time stress profiles as they are generated within the coating, as shown in Figure 14.

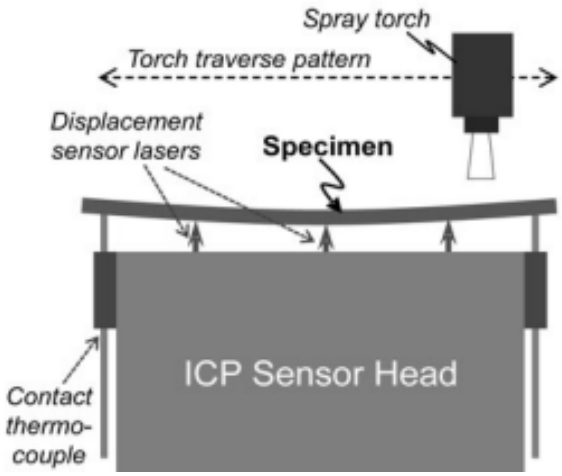

Figure 14. ICP setup showing beam and raster pattern

To record ICP data in the CAPS vacuum chamber, modified passthroughs were created to keep the DAQ and computer with the ICP software outside. K-type thermocouples were used to rewire the displacement lasers to an existing thermocouple passthrough and back to the Data Acquisition box (DAQ), and ICP thermocouples were connected to the CAPS system thermocouples. Data was collected separately for substrate temperature and displacement and recombined post-spray from the two separate DAQ's. Beam mass and thickness were measured pre- and post-spray to record the deposition. Two preheat passes with no powder were sprayed over the beam followed by 10 passes with powder. The spray torch was programed for a lateral movement across the length of the beam, in a 5 mm step size, at 500 m/s raster speed.

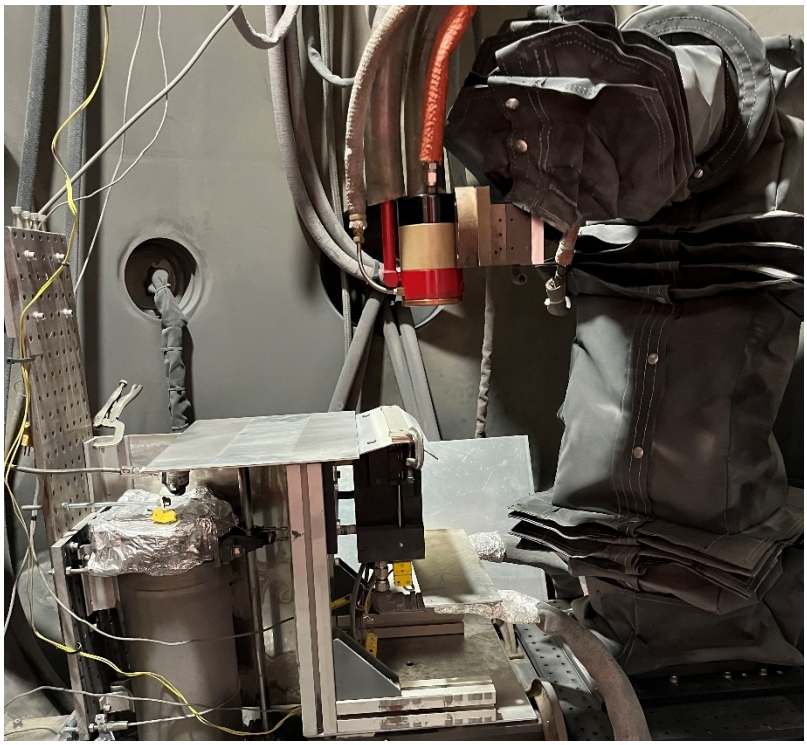

Figure 15. ICP placed in CAPS, with the torch mounted on a 6-axis Fanuc Robot

Chapter 4
Results

4.1 Chemistry Preservation with CAPS and Masking

Chemical analysis was performed for both powder feedstock and fabricated coatings to validate the chemistry preserving properties of CAPS when compared to air sprayed coatings. Powders analyzed prior to deposition are shown in Table 6. Low weight percentages of oxygen and nitrogen indicate high purity metals.

Table 6. LECO Interstitial Analysis for Oxygen and Nitrogen Content in Powder Feedstocks

Sample	Concentration of Oxygen (wt%)	Concentration of Nitrogen (wt%)
HC Starck Tantalum	0.0439 ± 0.0072	0.0696 ± 0.0207
Praxair Nickel	0.01873 ± 0.00075	0.00787 ± 0.00030

Oxygen and nitrogen contents obtained from the LECO analysis were compared to a control sample of air sprayed tantalum. Nickel is much less reactive than tantalum under plasma spray environments, and thus samples were fabricated in CAPS to note the oxygen and nitrogen contents. The total oxide content in CAPS tantalum was reduced by 94.5% in comparison to the sample sprayed with APS. When compared to the original powder chemistries alongside the air sprayed samples, tantalum purity is very minimally affected, although some trace oxides are included (the powder chemical analysis was performed on different lots from those sprayed in the study, which may cause minor variance but is accepted as the same feedstock). Chemical analysis reinforces the use of CAPS for generated high-purity metallic coatings.

Table 7. LECO Interstitial Analysis for Oxygen and Nitrogen Content in CAPS vs. APS Samples

Sample	Concentration of Oxygen (wt%)	Concentration of Nitrogen (wt%)
Air Sprayed Tantalum	1.6578 ± 0.0153	0.2370 ± 0.0047
CAPS Tantalum	0.0916 ± 0.0095	0.0942 ± 0.0395
CAPS Nickel	0.0252 ± 0.0012	0.0806 ± 0.0072

4.2 Substrate Temperature

4.2.1 Differential Flame Thermometry

IR images of the DFT front plate during testing of the same torch condition with and without plume quenching is shown in Figure 16. With the plume quench off, a nearly symmetrical temperature profile about the approximate center of the DFT front plate is observed. With the

plume quench on, a visually apparent skewing of the temperature profile and change in location of the peak temperature on the front plate is observed, offering strong evidence that the hot plasma gases are being re-directed by the plume quench.

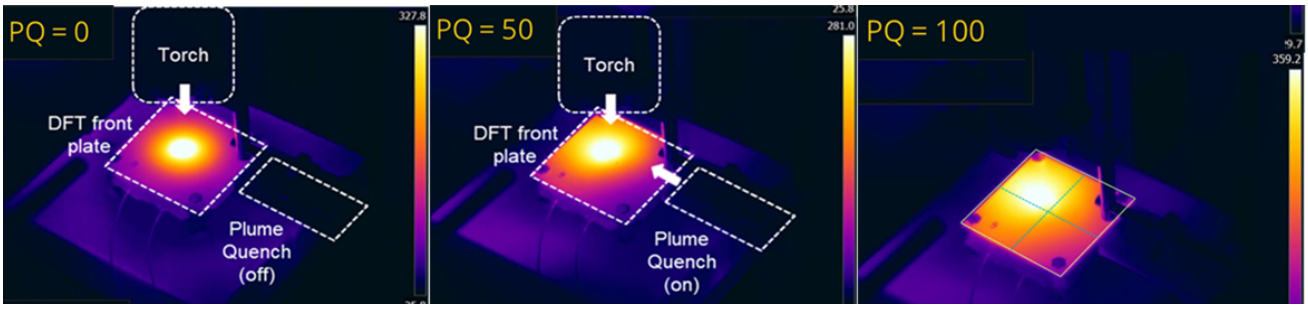

Figure 16. Differential Flame Thermometry images showing the configuration within the CAPS chamber with the torch set with and without plume quenching at 0, 50, and 100 slpm.

Substrate temperature profiles were observed using the DFT described in section 3.1.2 Differential Flame Thermometry as a preliminary "proof of concept", and captured as diffused temperature data and IR images. DFT data is typically used to calculate a one-dimensional heat flux by using the properties within its construction (e.g. layer thicknesses, material heat capacities) and temperature measurements of the front and back Inconel plates during testing. However, the spatially varied temperature profile (i.e. two-dimensional as opposed to one-dimensional) on the DFT front plate observed in Figure 16 means that any heat flux calculation made in this way with the experimental data from these tests would not be valid. Instead, the temperature measurements of the DFT backplate were studied to infer the relative effects on the plume quench; it is assumed that the spatial temperature distribution of the DFT backplate is more uniform since the absorbed heat flux conducts through the front plate and thick insulator layer to reach the back plate. DFT back plate temperature data from a subset of the test series using the SN-Low condition and different plume quench parameters are given in Figure 17 as an example. For each test series the plume quench flow rate was 0, 50, or 100 slpm. The plume quench was applied either while the torch was on and facing the DFT front plate (from time 0-600 seconds), the torch was off (from 600 seconds to the end of the data), or both. Each temperature series is labeled according to plume quench flow rate while the torch was on and then off.

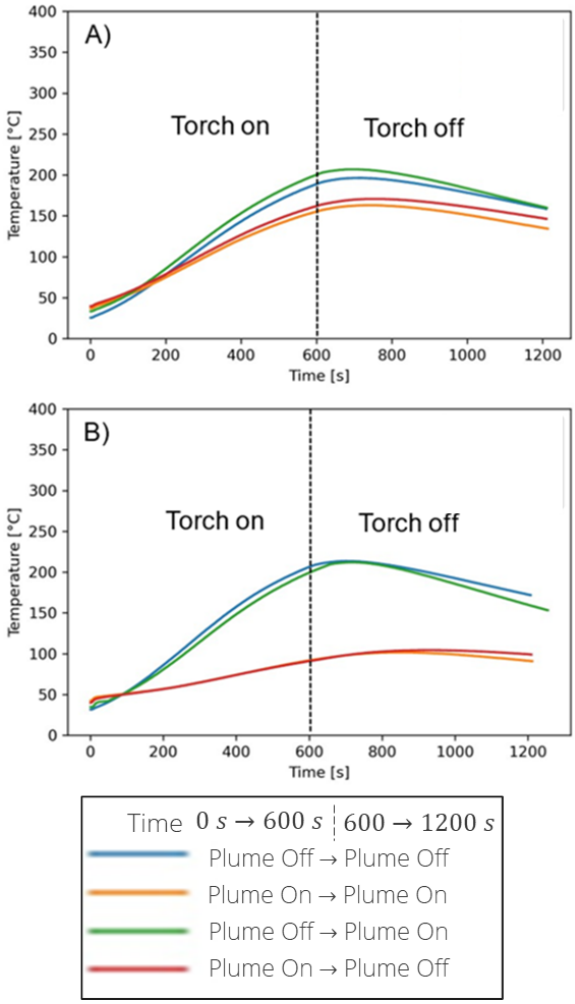

Figure 17. Backplate substrate temperatures measured with the DFT for plume quenching at A) 50, and B) 100 slpm where plume quenching flow rate pattern is described before and after 600 seconds of torch time.

The data series presented in Figure 17 provides further insight into the effect the plume quench has on the hot gas plume and subsequent substrate heating as well as the plume quench's direct cooling of the substrate after the torch is extinguished. When used while the torch is on and the back plate temperature rises (0 to 600 seconds), a plume quench flow rate of 50 slpm (orange and red data series in Figure 17) results in a lower DFT backplate temperature compared to when the plume quench is not used (0 slpm, blue and green data series in Figure 17). A substantially lower temperature during heating is measured when a flow rate of 100 slpm (orange and red data series) is used for the plume quench (Figure 17). This observation supports the hypothesis that the plume quench reduces the heat imparted onto the substrate surface by the hot plasma gases.

Furthermore, a dependance on the plume quench flow rate to this effect is also apparent. When the torch is extinguished and the back plate temperature decreases after a short delay (600 seconds to the end of the data), the plume quench seems to have a minor effect where the DFT back plate temperature decreases at a slightly faster rate for 50 and 100 slpm compared to when the plume quench is not used (0 slpm). The rate of temperature decrease does not appear to be strongly dependent on the plume quench flow rate. IR imaging during cooling did not indicate an obvious temperature profile change on the DFT's front plate was produced by the plume quench.

4.2.2 In-Situ Curvature Properties Substrate Temperature

Beam temperature is one of the variables measured with the In-Situ Curvature Properties sensor described in section 3.4.3 Residual Stress Measurements, which was isolated to compare substrate temperatures (measured on the backend of the beam) throughout deposition. As shown in Figure 18, the peak substrate temperature for all substrate-coating pairing decreases with the addition of plume quenching. This furthers the evidence in section 4.2.1 Differential Flame Thermometry, which showed reduction in diffused substrate temperature and change in heat gradient.

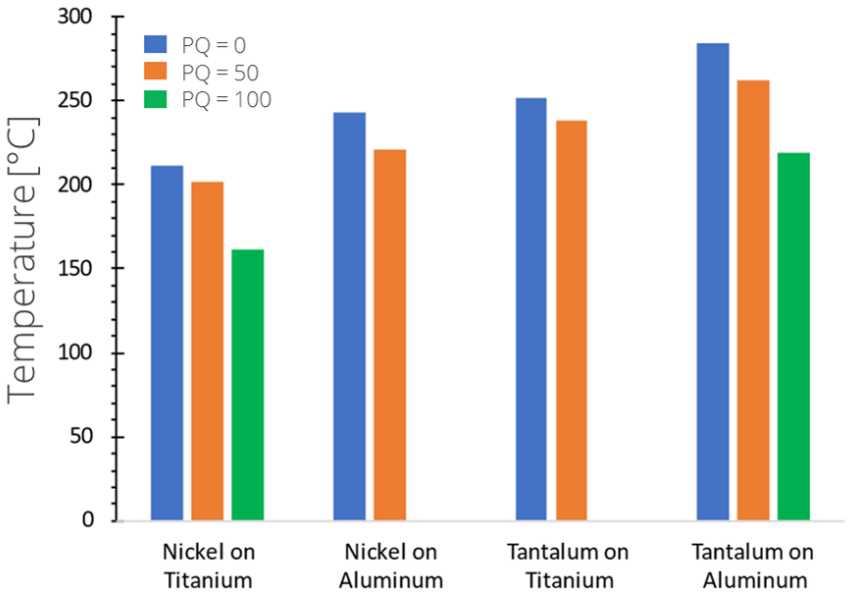

Figure 18. Peak substrate temperatures for all substrate-coating pairs and plume quenching conditions taken during ICP measurements described in section 3.4.3 Residual Stress Measurements.

The substrate temperatures measured on the backside of the ICP beam were plotted against each other for each plume quenching condition. Tantalum on aluminum and nickel on titanium were two pairings that were measured at all three plume quenching conditions (0, 50, 100) to probe the differences in final stress states for the largest negative CTE difference (tantalum on aluminum, Δα = -17) and for the only positive CTE difference (tantalum on aluminum, Δα = 5.5). Tantalum on aluminum ($\alpha_{substrate} > \alpha_{coating}$) will generate a compressive residual stress state (Δα), while nickel on titanium ($\alpha_{substrate} < \alpha_{coating}$) will generate a tensile stress state (Δα).

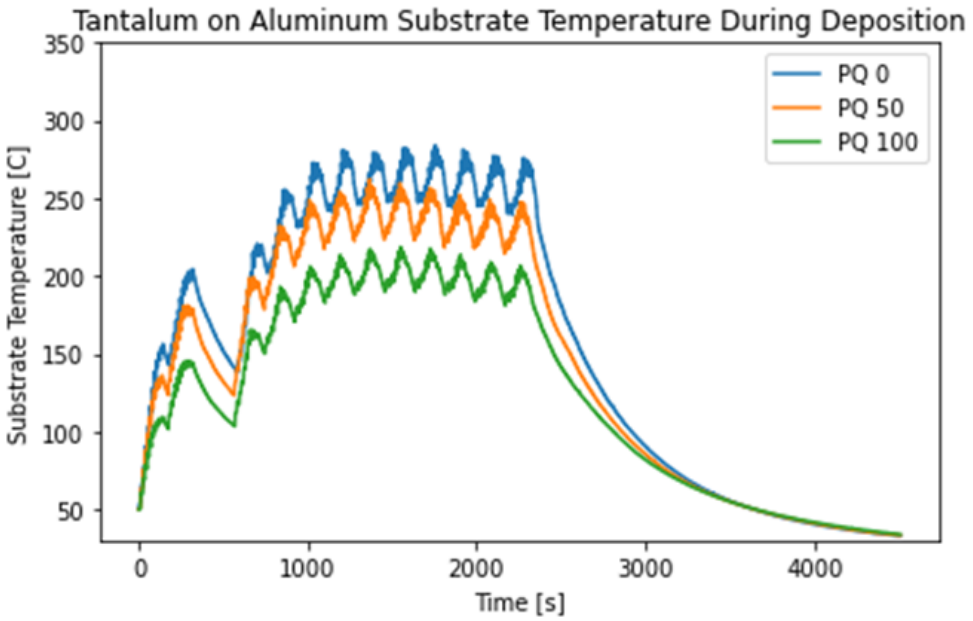

Figure 19. Substrate temperatures for tantalum on aluminum for plume quenching conditions of 0, 50, and 100 slpm

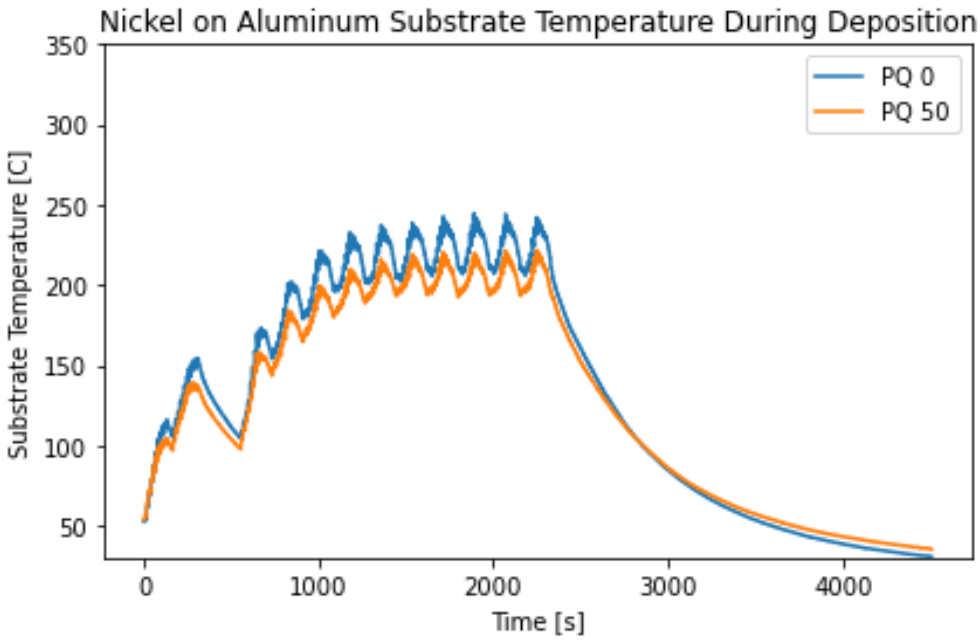

Figure 20. Substrate temperatures for nickel on aluminum for plume quenching conditions of 0 and 50.

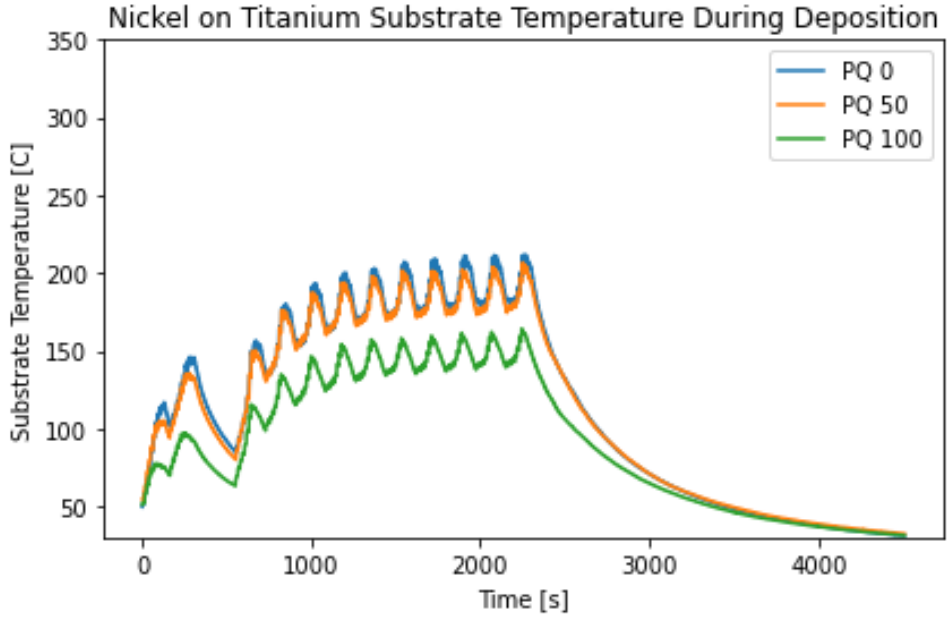

Figure 21. Substrate temperatures for nickel on titanium for plume quenching conditions of 0, 50, and 100 slpm

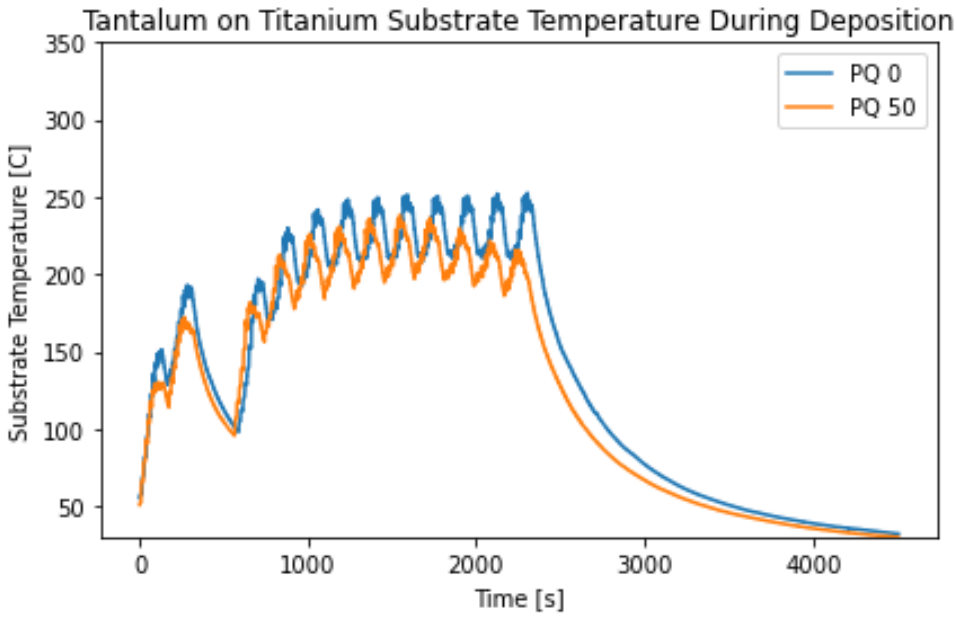

Figure 22. Substrate temperatures for tantalum on titanium for plume quenching conditions of 0 and 50

While peak temperatures change with material combination, there is a consistent trend in substrate temperature reduction seen in all samples.

4.3 Plume and Particle Measurements

4.3.1 Powder Feedstock

Nickel and tantalum powders were analyzed for particle size and distribution using the Beckman Coulter PSA system described in section 3.2.1.1 Particle size and chemical analysis. SEM images were also taken to show morphology.

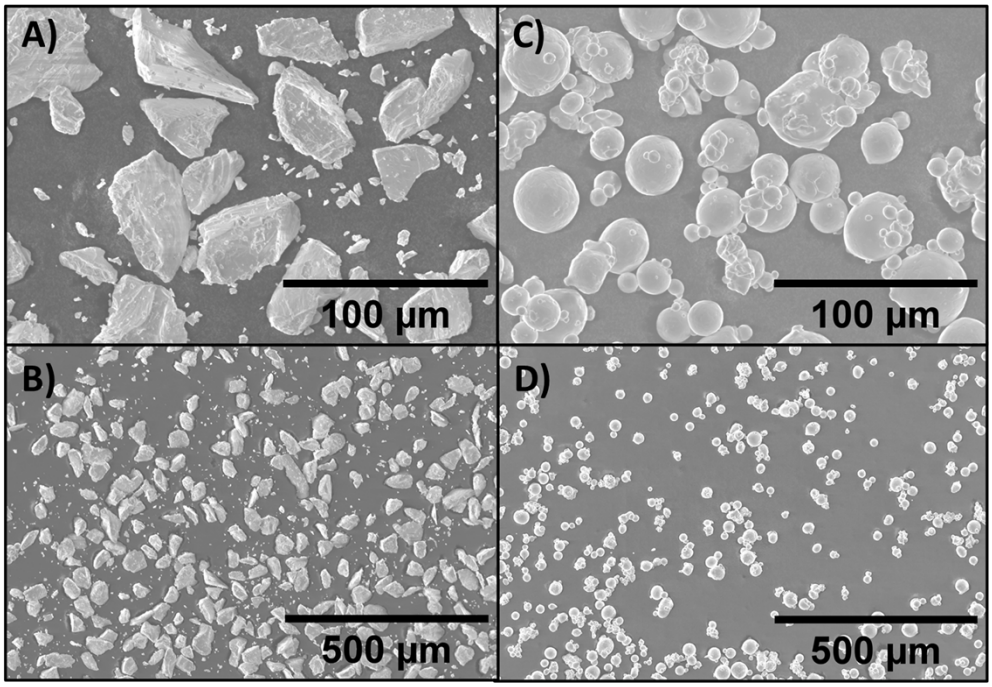

Figure 23. SEM images taken of tantalum (A, B), and nickel (C, D) feedstock powders.

The SEM images in Figure 23 show general agreement in particle size, with some fines included in the tantalum powder (Figure 23-A, B) that don't visually appear in the final coating microstructure. Particle size analysis was performed three times for three powder samples, and the average values are reported in Table 8. The three repeated runs for particle size measurement for each powder are shown in Figure 24 and Figure 25, and are reported by occurrence in volume percent. The particle size distribution is contained between 10-100 µm for both feedstocks (with the exception of the fine particles in the tantalum), and although the nickel spread is narrower the means between both materials are within one standard deviation of each other shown in Figure 26.

Table 8. Particle Size Analysis for Nickel and Tantalum Feedstock

Powder	Mean (µm)	Standard Deviation (µm)	Morphology
Nickel (Praxair Ni-914-13)	38.11	10.72	Atomized
Tantalum (HC Starck)	43.51	13.82	Fused and Crushed

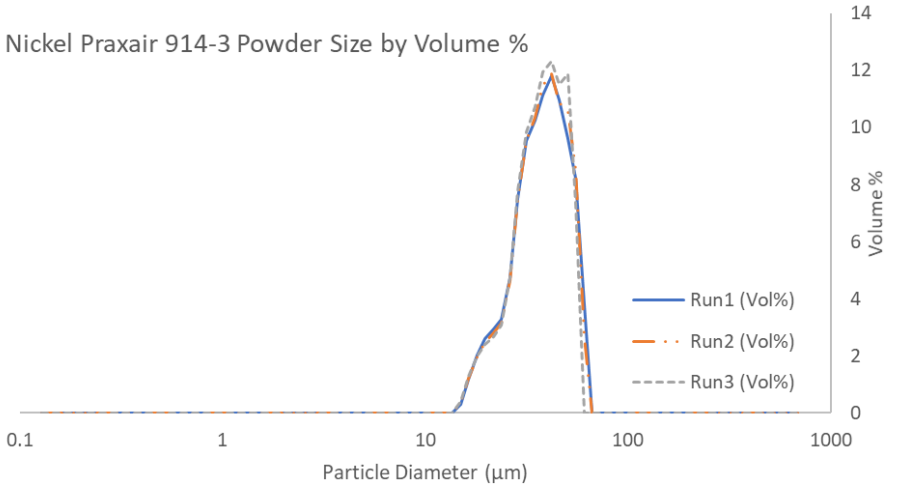

Figure 24. Nickel powder particle size distribution

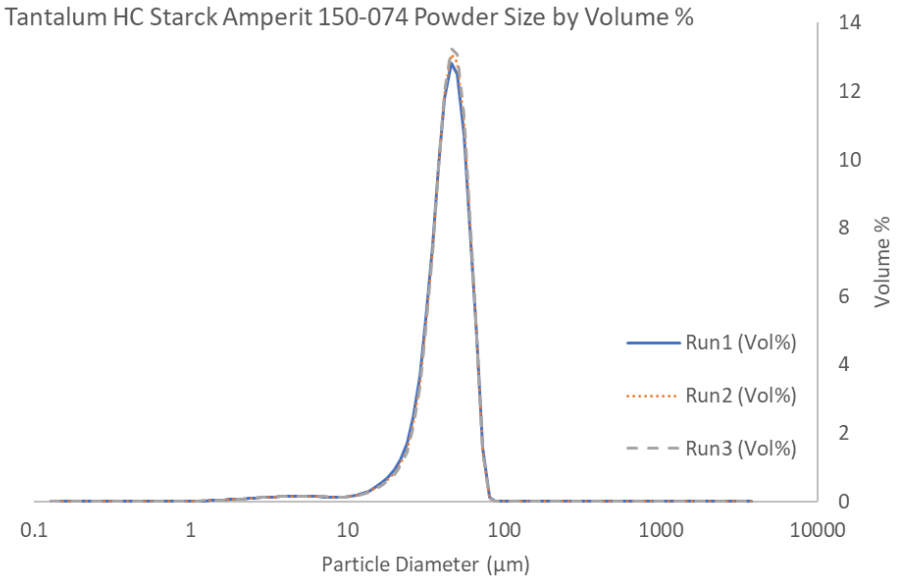

Figure 25. Tantalum powder particle size distribution

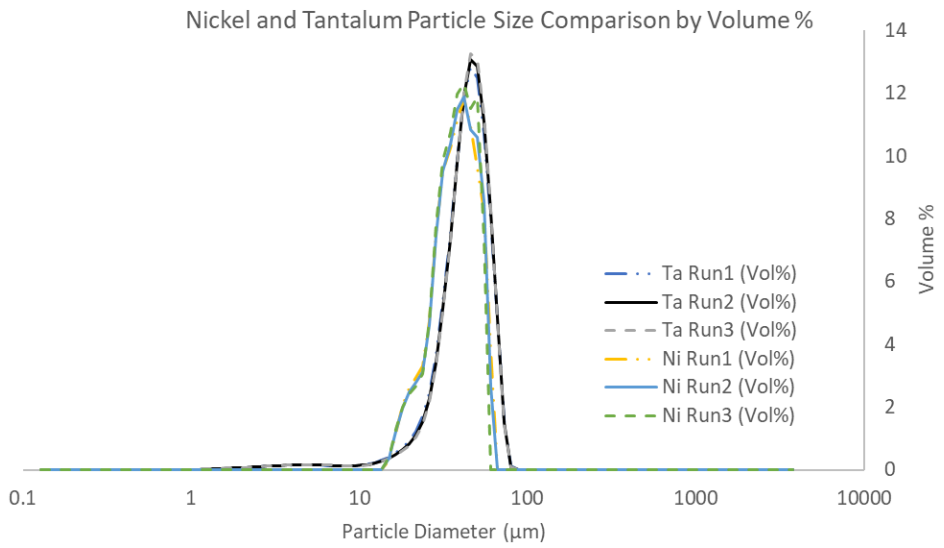

Figure 26. Powder feedstock particle sizes compared for nickel and tantalum

The powder feedstock particle size overlaps seen in both Figure 26 and when looking at the distribution with error in Table 8.

4.3.2 Plume Diagnostics

Plume diagnostics were measured at three spray distances with three plume quenching flow rates (0, 50, and 100 slpm). Particle velocity and temperature were measured for tantalum and shown in Figure 27 andFigure 28, respectively. Particle velocity shows minimal change with the addition of plume quenching at 50 and 100 slpm and show little variation with spray distance. Reported errors for all conditions are within approximately 10 m/s of each other, showing that any influence of the plume quenching is within the same spread and not causing a significant difference.

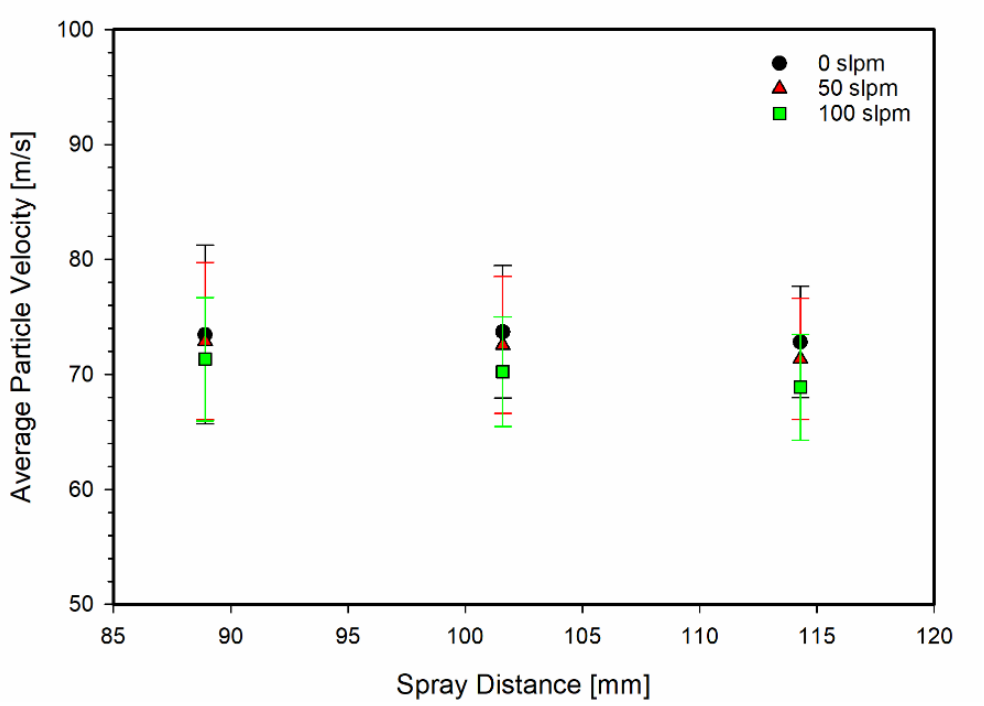

Figure 27. Average particle velocity for tantalum within the plume measured for 60 seconds at quenching conditions of 0, 50, 100 slpm.

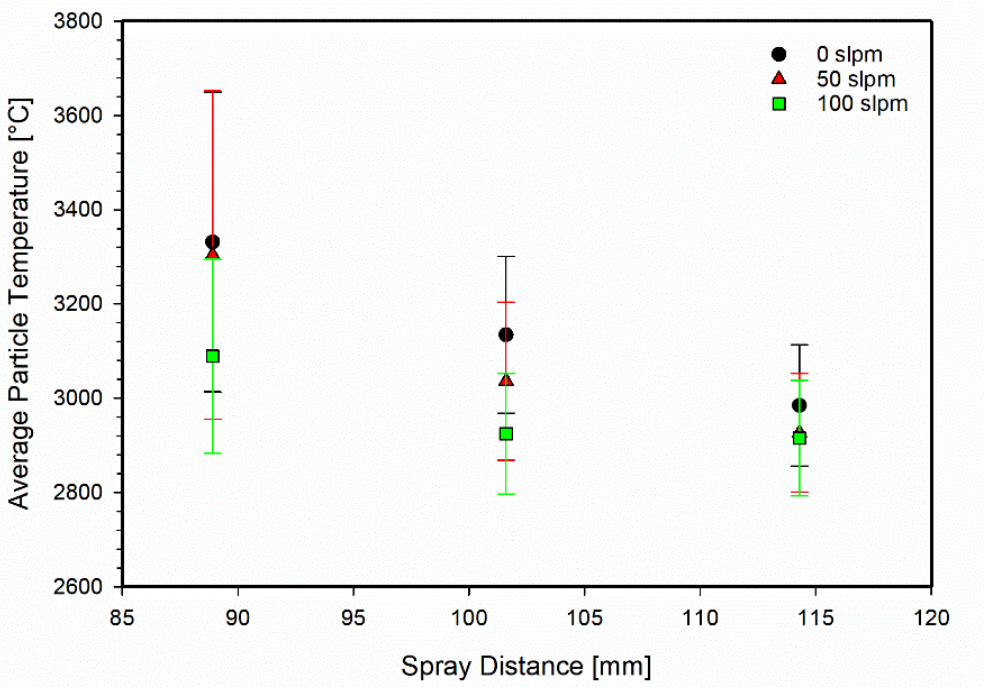

Figure 28. Average particle temperature for tantalum within the plume measured for 60 seconds at quenching conditions of 0, 50, and 100 slpm.

4.4 Deposition Efficiency and Properties

4.4.1 Volume, mass, button study

Eight buttons were fabricated for each coating-substrate pairing for plume quench conditions of 0 and 50 slpm to investigate the effect on coating deposition. Buttons were measured before and after deposition to find coating thickness and deposited mass (shown in Figure 29), which were used to calculate the coating density volumetrically (shown in Figure 32).

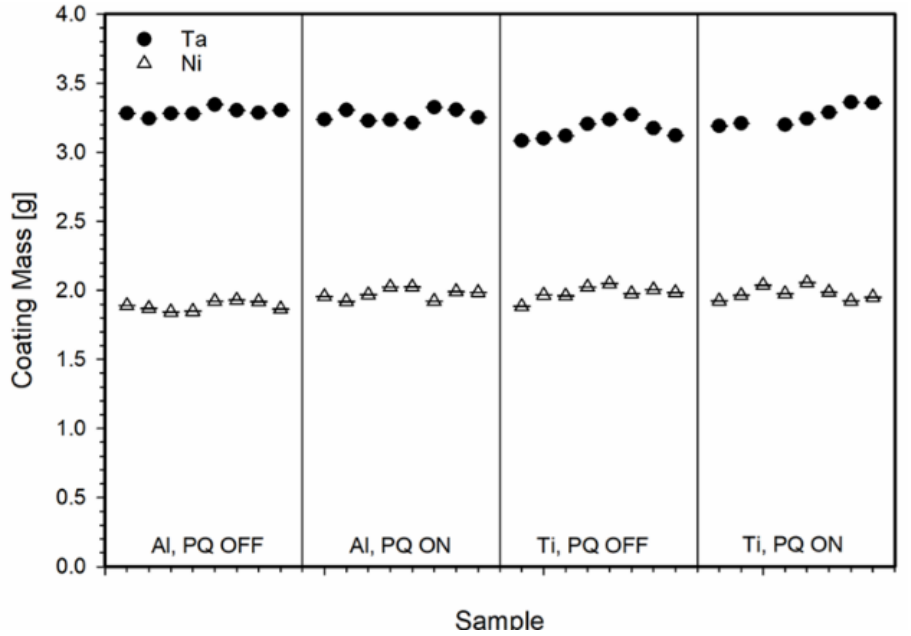

Figure 29. Measured coating mass for all coating and substrate pairings on button samples.

Coating masses are shown for tantalum and nickel coatings side by side for all substrates and plume quenching conditions (PQ OFF being 0 slpm, and PQ ON being 50 slpm), and based on spindle spoke position (1-8). There is very good agreement in coating mass between all plume quenching conditions and substrates, which reaffirms that plume quenching does not affect deposition efficiency.

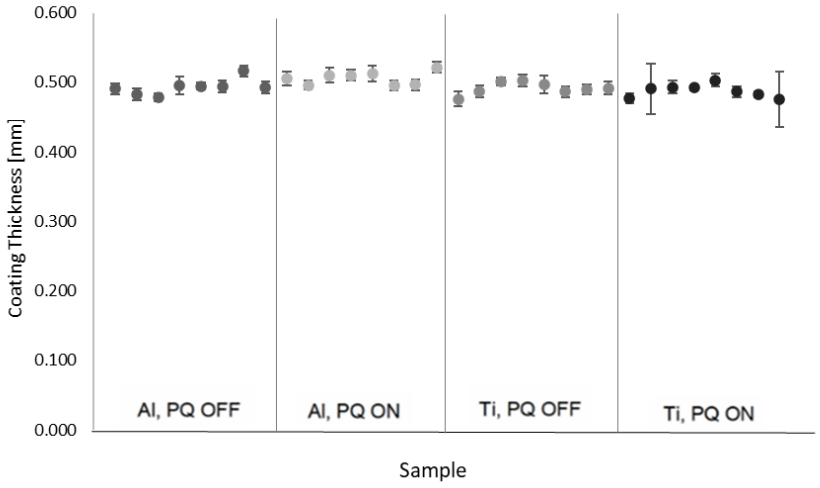

Figure 30. Nickel coating thickness after deposition

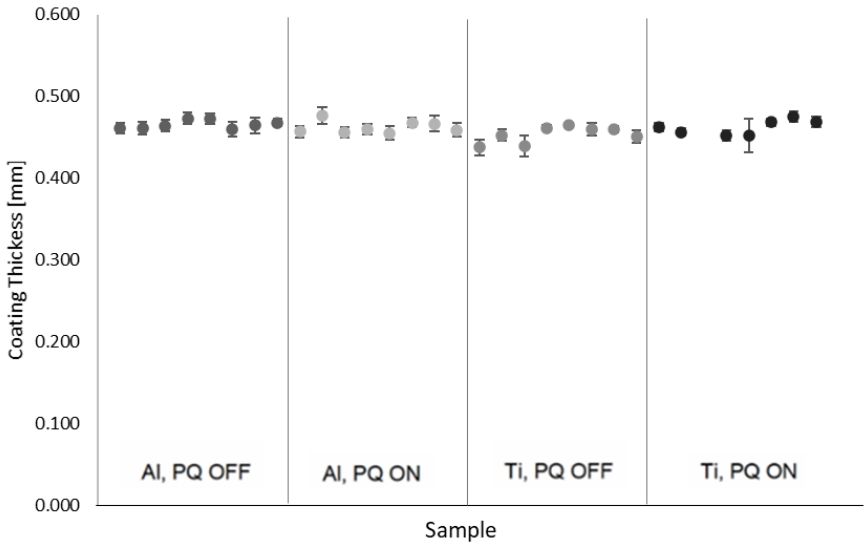

Figure 31. Tantalum coating thickness after deposition

Average coating thicknesses measured with a ball micrometer (shown in Figure 30 and Figure 31) show consistency in thickness with minimal error for multiple measurements for each sample (taken with a ball micrometer with 0.001 mm precision).

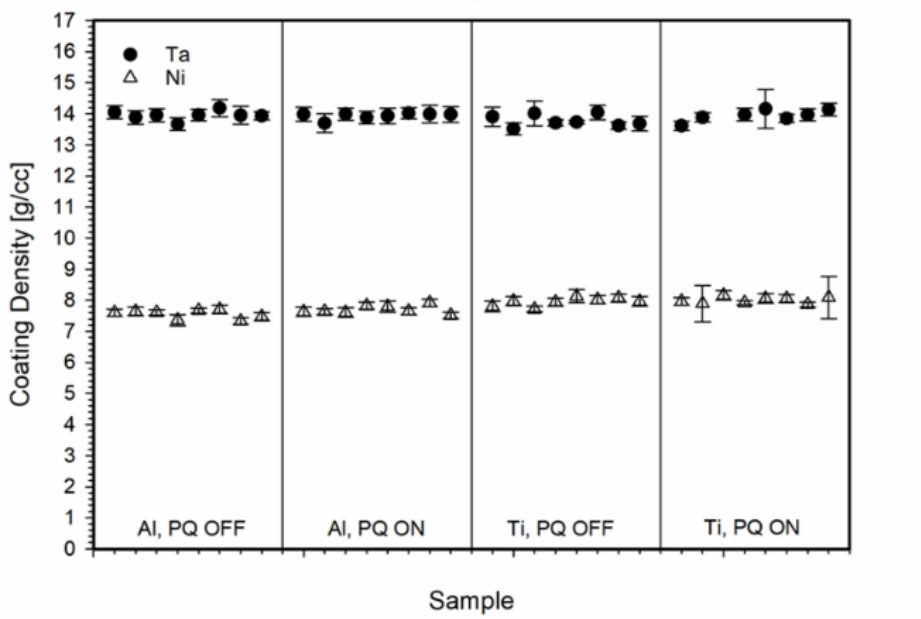

Figure 32. Measured coating density for all coating and substrate pairings on button samples.

Coating density was calculated volumetrically using the measured thicknesses and reported with error. As expected, similar button masses and thicknesses generate similar coating densities. This continues to reaffirm that the addition of a plume quench at 50 slpm does not cause any significant effect on the coating deposition.

4.4.2 Microstructure

Microstructure was imaged using an SEM after metallographic preparation, and images were used to measure coating porosity. Microstructure was measured for both nickel and tantalum coatings. Microstructure reflects particle temperature and velocities and can show any immediately distinctive structural differences.

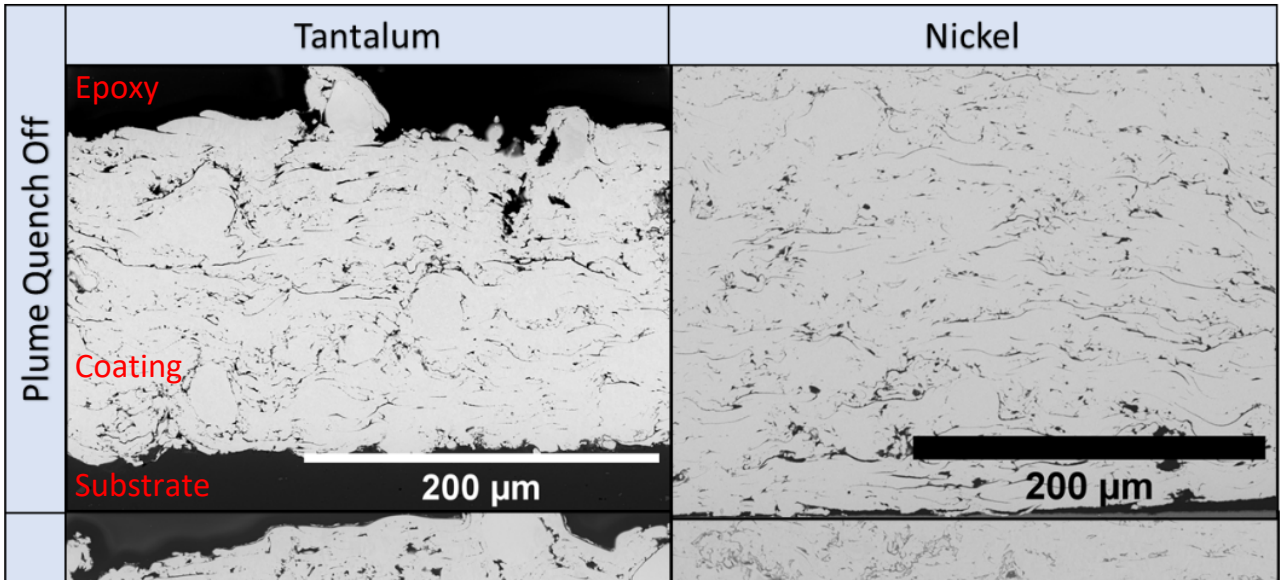

Figure 33. Coating microstructures for tantalum and nickel with and without plume quenching at the 100 mm spray distance.

Tantalum and nickel coatings are shown in Figure 33 with and without plume quenching at the same magnification. Similar microstructures are seen between the two samples, indicating similar (unaffected by plume quenching) particle temperature and velocity. Tantalum cross sections were taken from all bilayer beams used for thermal cycling (shown in Figure 8-B), while nickel cross sections were taken from two randomly selected buttons (one without and one with plume quenching).

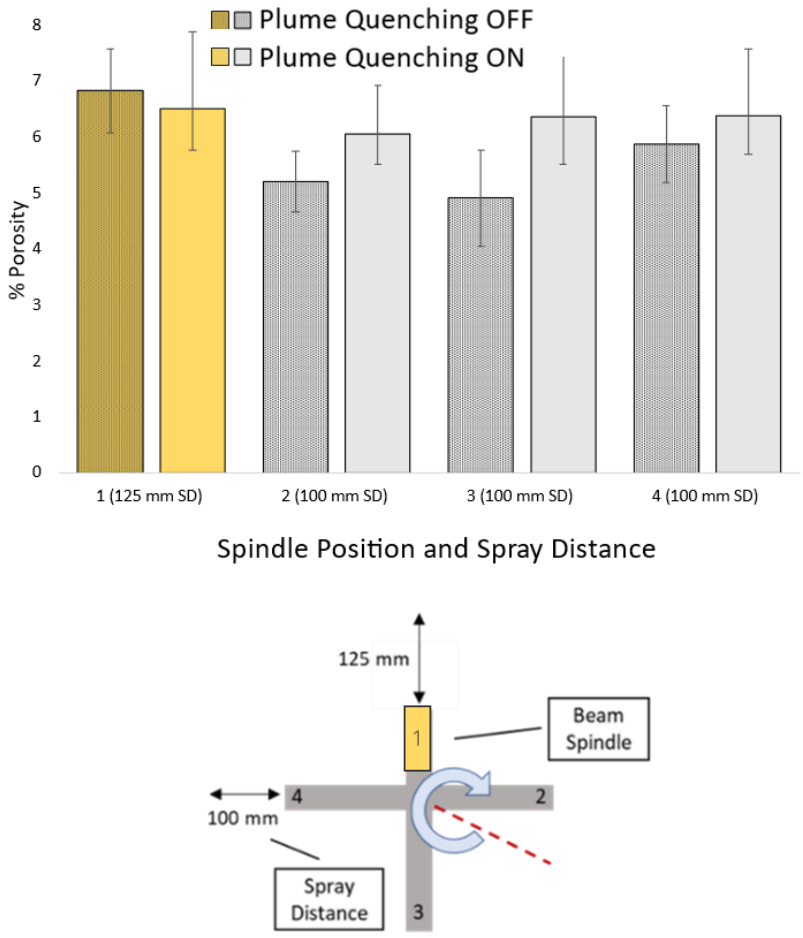

Figure 34. Image analysis porosity for tantalum based on spindle position and spray distance.

The porosity was measured as an average value for each beam sprayed on the spindle, including the beam placed at a larger spray distance as shown in Figure 34. There is some minor increase in porosity with the addition of plume quenching for tantalum, but all values fall within the error of both conditions between all beam conditions. The porosity was also measured for nickel as 4.8 ± 0.15% and 5.2 ± 0.2% as an average of multiple images from the same cross-sectioned sample.

4.5 Tensile Adhesion Testing

The tensile adhesion testing was performed and reported for tantalum and nickel coatings on titanium substrates. Coatings deposited on aluminum substrate created variable and unusable

adhesion results, which was characterized by mixed failure where failure occurred both in the adhesive as well as partially in the coating.

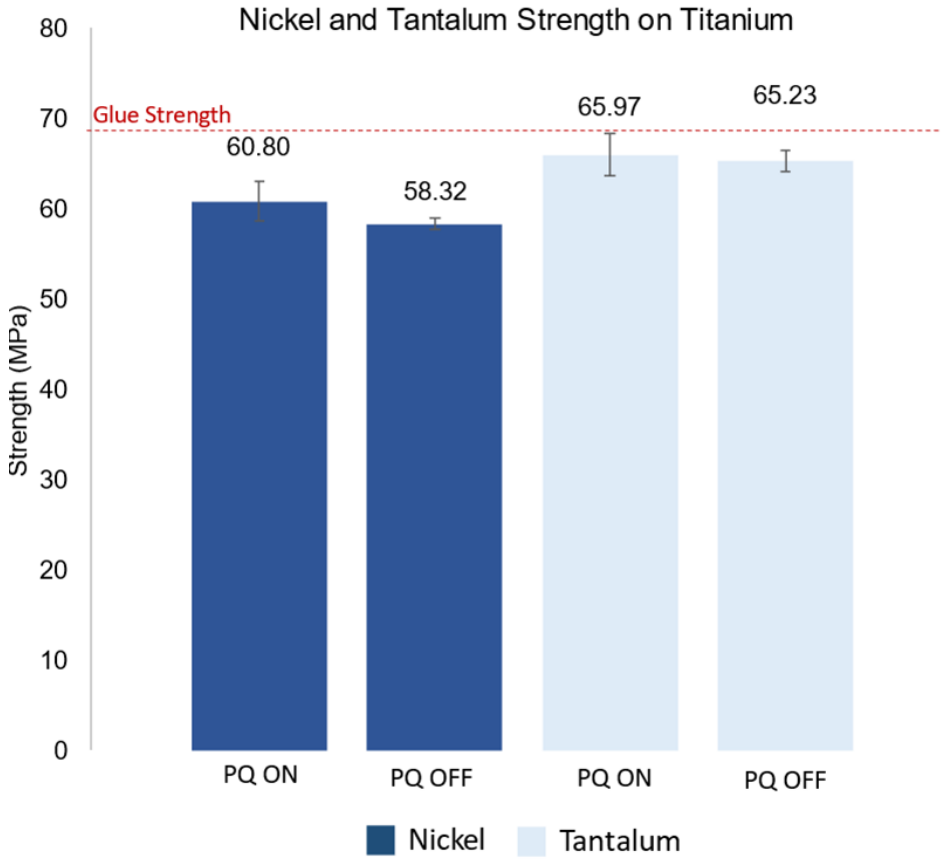

Figure 35. Tensile adhesion testing for nickel and tantalum on titanium substrates.

The results are reported alongside a "Glue Strength", which is measured using bare samples alongside each coated sample set to verify the integrity of the adhesive. Each coating-substrate condition result with and without plume quenching is the average of five pulled samples, and the reported glue strength for nickel and tantalum plots is the average of all ride along glue tests (one for each set of plume quench off and on).

4.6 Bilayer Beam Cycling for Coating Modulus

Thermal cycling was performed for a total of eight tantalum on aluminum beams, half with plume quenching at 50 slpm. The spindle fixture contained all four beams for each condition, with one at a slightly larger spray distance shown in Figure 36. The final calculated modulus is shown for each beam with respect to its position on the spindle, shown in Figure 36.

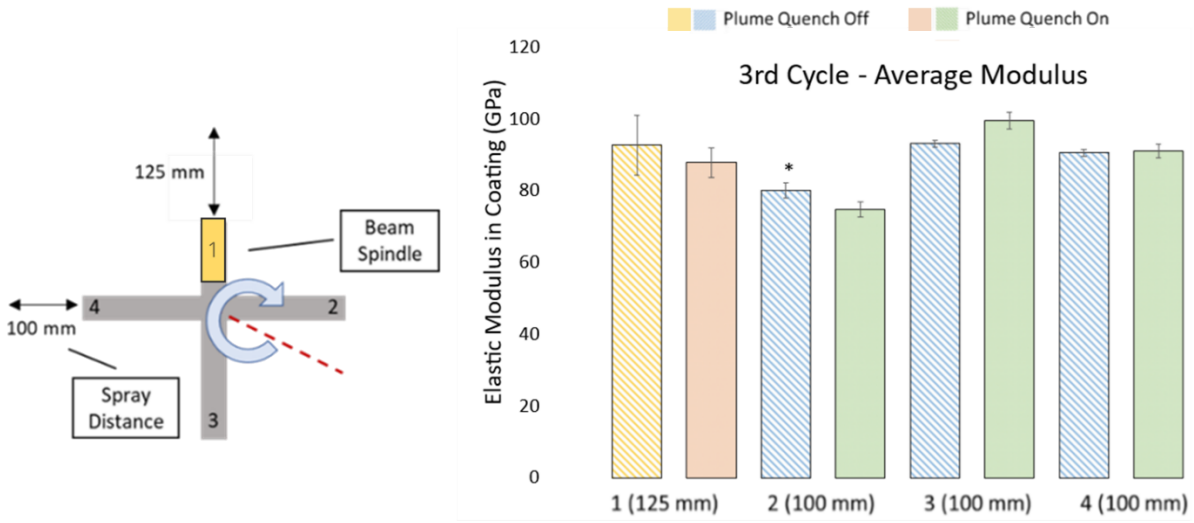

Figure 36. Coating modulus measured for the third thermal cycle, reported by spindle position

The reported modulus for the beam in position 2 without plume quenching (noted as *) is taken from the second cycle due to hardware malfunction during thermal cycling during the third cycle. This result is accepted as valid, as the second and third cycles are typically more uniform after thermal shakedown from splat sliding and stress relief occurring in the first cycle.

4.7 In-Situ Coating Residual Stress Measurements

The In-Situ Coating Properties (ICP) sensor was used to measure the live residual stresses as they develop in the coating during deposition. Using Equation 2, the measured curvature, temperature, and difference in CTE are used to calculate the thermal and deposition components of residual stress in each coating. The deposition and thermal stress are shown, as well as their compounded residual stress, and evolving stress (the growth of stress within the coating) in Figure 37.

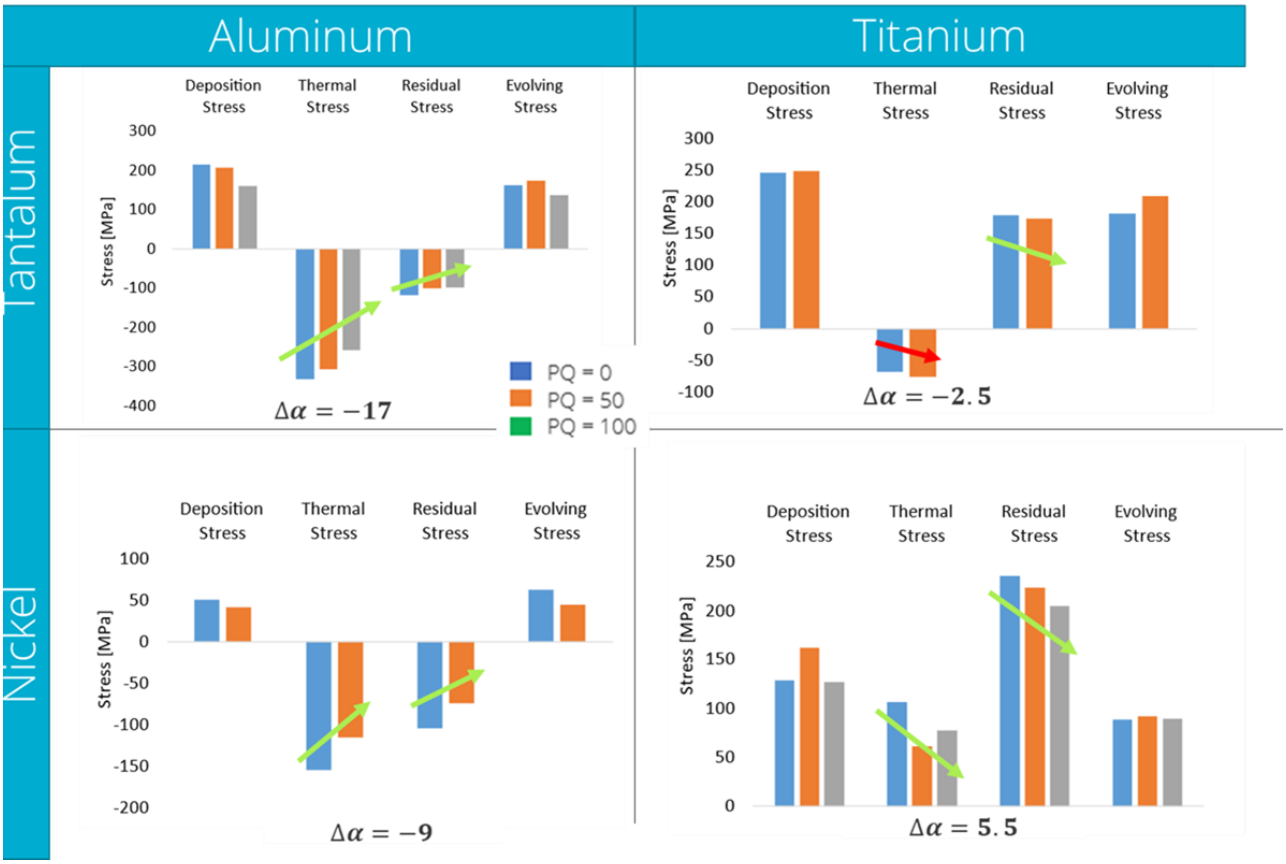

Figure 37. Stresses measured with ICP sensor for all coating and substrate pairings with plume quenching at 0, 50, and 100 for some pairings. The difference in CTE (Δα) between coating and substrate is shown for each pairing.

Stresses were measured for all coating and substrate pairings at 50 slpm, and 100 for tantalum on aluminum and nickel on titanium. The higher plume quench flow rate was investigated to probe CTE mismatch differences, with tantalum and aluminum having the largest negative mismatch (-Δα) and nickel and titanium having the only positive mismatch (+Δα). The individual residual and thermal stresses are shown for each pairing in Figure 38, Figure 39, Figure 40, and Figure 41.

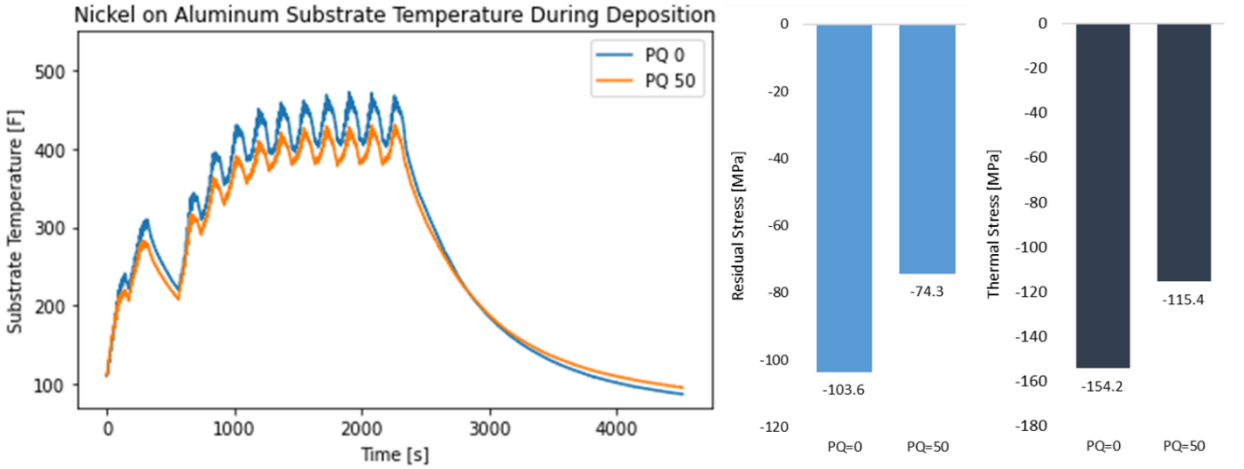

Figure 38. Residual stress and substrate temperatures for nickel on aluminum coating-substrate pairing.

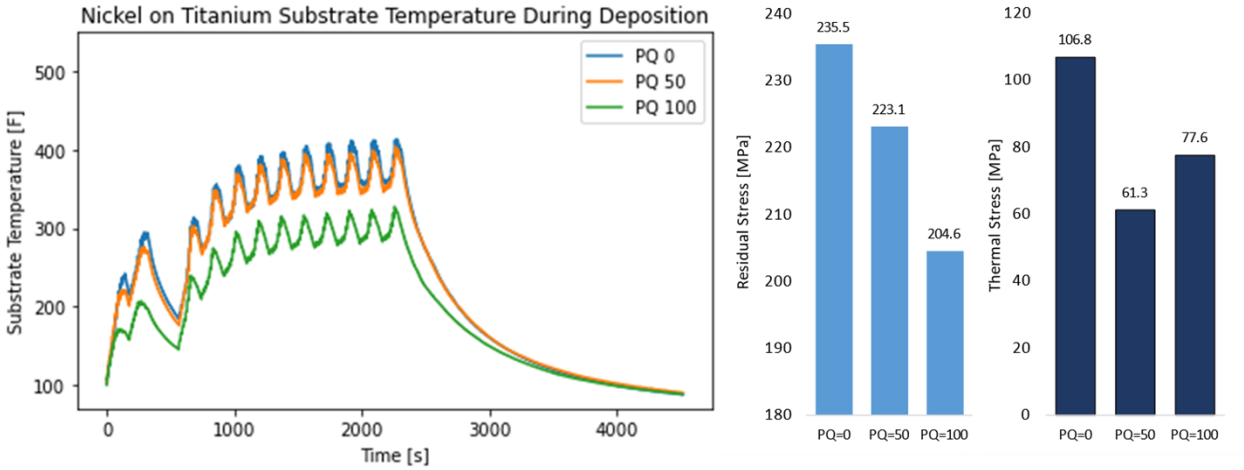

Figure 39. Residual stress and substrate temperatures for nickel on titanium coating-substrate pairing

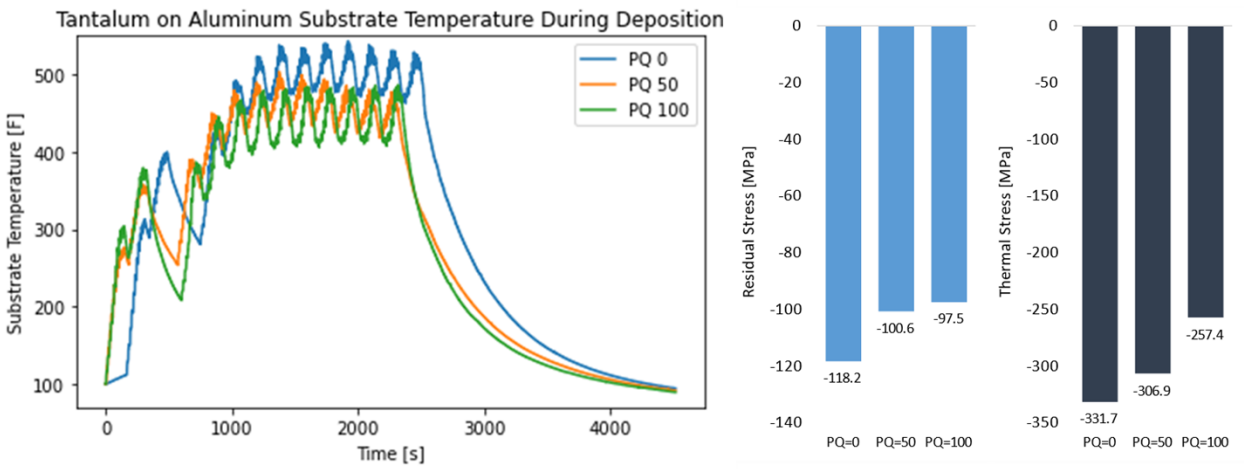

Figure 40. Residual stress and substrate temperatures for tantalum on aluminum coating-substrate pairing

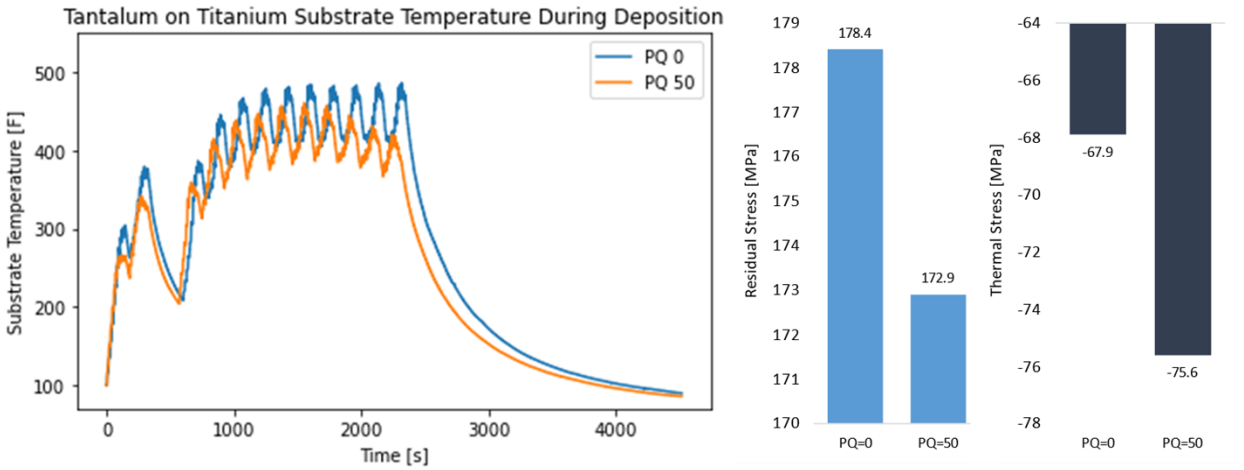

Figure 41. Residual stress and substrate temperatures for tantalum on titanium coating-substrate pairing

All stresses are also reported in Table 9 as the thermal and deposition counterparts, and the combined residual stress. Negative thermal stress values are indicative of compressive final stress states, which are the result of negative CTE difference between the coating and substrate pairings, which occurs in three out of the four pairings apart from nickel on titanium (which results in a tensile thermal stress state).

Table 9. Residual stresses and their thermal and deposition counterparts for all coating-substrate pairings and plume quenching conditions.

Sample ID		Spray Condition	Deposition Stress [MPa]	Thermal Stress [MPa]	Residual Stress [MPa]
Nickel Coating	Aluminum Substrate	PQ = 0	50.6	-154.2	-103.6
		PQ = 50	41.1	-115.4	-74.3
	Titanium Substrate	PQ = 0	128.7	106.8	235.5
		PQ = 50	161.9	61.3	223.1
		PQ = 100	127	77.6	204.6
Tantalum Coating	Aluminum Substrate	PQ = 0	213.5	-331.7	-118.2
		PQ = 50	206.3	-306.9	-100.6
		PQ = 100	159.9	-257.4	-97.5
	Titanium Substrate	PQ = 0	246.3	-67.9	178.4
		PQ = 50	248.5	-75.9	172.9

Chapter 5

Discussion

5.1 Substrate Temperature Reduction

5.1.1 Plume Quench Effect Measured by Differential Flame Thermometry

The IR images shown in Figure 16 clearly show that the plume quench can successfully redirect the hot gases from a plasma plume, confirming the hypothesized effect of the plume quench. The diffused back plate DFT temperature data in Figure 17 strongly suggests that using the plume quench can reduce heat imparted onto a substrate by the hot plasma gases, and it appears that the plume quench does this by interacting with the hot plasma gases and not by independently convectively cooling the substrate.

The mechanism of heat reduction onto the substrate is not clear and may be a contribution of several factors. Assuming that all the heat was captured by the front plate of the DFT, re-direction of the hot gases alone would not reduce the overall heat imparted on the substrate surface[1]. Spreading the same amount of heat over a larger area could slow the rate of heat absorption into the substrate by decreasing the local temperature differential between the hot gases and substrate surface. The skewing of the DFT front plate temperature distribution (seen in Figure 16) and rate of temperature rise in the DFT back plate (seen in Figure 17) suggests that this plume quench driven heat spreading mechanism could be occurring.

Another mechanism that could be occurring is the quenching of the hot plasma gas by the cold plume quench gas. It is well known that the temperature of the plasma plume after exiting form the torch's nozzle decreases as the surrounding atmospheric gas mixes with and quenches the plasma gas plume [34]. At the distance the plume quench was placed from the torch nozzle exist in this study, the plasma gases can be considered recombined into monoatomic argon or argon/helium, which is visible as a limited observable light emission of the plume at this distance. In a non-ionized state, the molar heat capacity of argon (and helium) from room temperature to 6000 K is nearly constant [35] so any cold gas mixed into the plasma gases at this distance from the torch nozzle will be very effective in reducing the average gas temperature of the mixture, even more so than near the torch nozzle exit where the partially ionized argon has a much greater

[1] One could imagine where the plume quench would be a practical cooling technique for spraying a small substrate or workpiece where the hot gas plume could be redirected so that it largely avoids impinging onto the workpieces surface.

enthalpy content. The flow rates of gases used in the plume quenching are similar to those of the plasma gases, making it plausible that the mixture of cold and hot gases results in a gas with significantly lower heat content impinging on the substrate surface than without the plume quench. While the combination of dilution (plasma gas quenching and distributing) and deflection (the redirection caused by the bisecting cold-gas jet) are evident, the potential for improvement by pushing the redirected plasma gas entirely off of the workpiece would achieve an even greater cooling effect.

5.1.2 Substrate Temperature Measured During Deposition

The reduction in substrate temperature was initially measured as the diffused temperature on the back plate of the Differential Flame Thermometer (shown in Figure 17), which was taken with a stationary torch with plume quenching and without powder. Beam temperatures were later measured during the deposition for the residual stress measurements taken in section 4.7 In-Situ Coating Residual Stress Measurements) and compared for different plume quenching conditions.

There is a clear reduction in substrate temperature for all coating-substrate pairings that increases with plume quenching flow rate, which is expected as higher rates of plume quench flow are intended to redirect more of the hot gases before they can interact with the substrate. Peak substrate temperatures vary with the material combinations, but the general trend of substrate temperature reduction is always present, proving that plume quenching is a viable technique for reducing substrate temperature for the selected metallic pairings.

5.2 Coating Deposition Properties and Microstructure

Coating microstructure is a function of particle temperature and velocity, which vary based on the torch and spray conditions, and the imparted kinetic and thermal energy. Similar particle temperatures and velocities generate similar thermal spray microstructures. Particle temperatures and velocities were measured for tantalum powder between 0, 50, and 100 slpm to look for any interaction from the addition of the plume quenching gas jet.

5.2.1 The Effect of Plume Quenching on Particle Temperature and Velocity

The measured particle temperatures and velocities give us an idea of the effect of plume quenching on in-flight tantalum. Particle velocity (seen in Figure 27) shows minimal variation with both plume quenching and spray distance. The mean velocities measured for all plume quenching conditions at all distances varied no more than ~5 m/s in the maximum case (which was

found between the 0 and 100 slpm conditions taken at ~115 mm spray distance). The spread of error was also within approximately 10 m/s for all three conditions, showing that any effect of plume quenching on particle velocity was well within the reported error of the control group.

Particle temperature (seen in Figure 28) also showed minimal variation with the addition of plume quenching, although a decrease was noticed at the ~90 mm spray distance. The plume quench injection site is approximately 75 mm from the torch face, which was chosen because it is assumed that most of the particle heating and acceleration has already taken place at that distance. The decrease in particle temperature measured at the ~90 mm spray distance (approximately 15 mm from the plume injection site) was primarily apparent in the 100 slpm plume quenching condition. As the spray distance approaches 100 mm and 115 mm, the variation in average particle temperature decreased, and all values are within the experimental error of each other. The reduction in temperature spread as the measurement moves away from the plume quench injection site suggests that the plume quenching gas may be obscuring or interacting with particle temperature measurement at the injection site, but not actually affecting the particle temperature significantly.

5.2.2 Effect of Plume Quenching on Coating Deposition

The similar particle temperatures and velocities shown in section 4.3.2 Plume Diagnostics, indicate similar deposition and microstructural patterns. The deposition efficiency and density of both nickel and tantalum coatings was measured as the gain in mass and coating thickness, which showed highly consistent results for each material with and without plume quenching on both aluminum and titanium substrates. This indicates that the addition of plume quenching does not interact with the particles in the plume in a way that reduces or modifies the deposition efficiency, and coating density.

5.2.3 Microstructural Similarity in Plume Quenching Conditions

Microstructure reflects particle temperature and velocity and can show any immediately distinctive structural differences that would result from the addition of plume quenching. Figure 33 shows both nickel and tantalum coating cross sections with and without plume quenching at 50 slpm. On a visual basis, nickel and tantalum coatings do not show any outstanding anomalies with the addition of plume quenching condition. Both materials and conditions show the expected plasma sprayed microstructure, with a combination of well-melted particles, unmelts, and porosity.

Both nickel and tantalum coatings do not feature any vertical cracking and oxide stringers, indicating high purity deposits (typical to CAPS coatings fabricated in an inert argon environment). Looking at the cross sections side by side, it is hard to distinguish any visual differences, although additional material testing is necessary to validate similarity. For the purposes of comparison, compared samples were prepared at the same time using identical procedures, so while metallographic preparation may add an element of user error, the comparison is still valid.

Using the cross-section images for the tantalum and nickel coatings, porosity was calculated using the Multi-Otsu method described in section 3.3.2 Image Analysis. All tantalum beams fabricated for the bilayer thermal cycling technique were imaged and average porosity taken, including the larger spray distance sample shown in Figure 34. The porosity was shown as a function of the spindle position and as an average value for a set of 10 images taken from each sample. There is a minimal increase in porosity for the 100 mm spray distance samples, although the values sit within each other's reported errors. When comparing the porosity with spindle position, there appears to be more variation with the spindle position (1, 2, 3, and 4) than with the plume quenching condition.

5.3 Effect of Plume Quenching on Nickel and Tantalum Adhesion on Titanium

Adhesion was performed for nickel and tantalum samples on titanium substrates. Testing was attempted for aluminum substrates but resulted in inconclusive failure, potentially due to insufficient surface preparation. For the titanium substrates, all adhesion tests (for both nickel and tantalum samples) resulted in failure occurring within the adhesive. Tested sample failure occurred at close to the measured glue strength; adhesive strength was taken by pulling apart two glued adhesion slugs (such as those seen in Figure 9) without the sample button in between. The adhesive failures for both coatings tested at close to the glue strength; slightly lower results may be due the different configuration (the inclusion of sample button between adhesion slugs).

While failure occurring within the adhesive is not an indicator of bond strength between the coating and the substrate, it can be interpreted as a lower boundary for coating bond strength. To test adhesion strength, a stronger adhesive would be needed to exceed coating bond strength. Such adhesives exist, such as Master Bond epoxy, although unlike the standardized FM 1000 adhesive slips it requires manual application of the epoxy paste which is not well calibrated. For the range

of adhesion strength examined, plume quenching was determined to have no effect on both nickel and tantalum coatings.

5.4 Effect of Plume Quenching on Tantalum Coating Modulus

Coating modulus was measured using bilayer thermal cycling and the resulting modulus for tantalum samples is shown in Figure 36. After three cycles, it is assumed that curvature behavior stabilizes (because of initial splat sliding and relaxation) and can be used to calculate coating modulus. Modulus was measured for all spindle positions, one of which is at a slightly larger spray distance. The variability between the plume quenched condition for each spindle condition is low (e.g., position 1 with and without plume quenching), and variability between the positions themselves is greater. Spray distance also does not show a significant difference with the addition of plume quenching when compared to the other spindle positions at 100 mm spray distance. As expected from the similar coating microstructure shown previously, the coating modulus does not vary substantially, further establishing that plume quenching at 50 slpm does not alter the coating.

5.5 Residual Stress Reduction from Plume Quenching

There is a strong relationship between substrate temperature, CTE mismatch, and thermal stress. The residual stresses were measured for tantalum and nickel coatings on titanium and aluminum substrates by measuring curvature and temperature response during deposition. Residual stresses are compounded from thermal and deposition stresses, which are formed by CTE mismatch and rapid particle quenching, respectively. For the four different substrate-coating pairings, CTE mismatches ($\Delta\alpha$) are shown in Figure 37. Except for nickel on titanium, all $\Delta\alpha$ are negative causing a compressive thermal stress. Nickel on titanium has a positive $\Delta\alpha$, which results in a tensile (positive) thermal stress state.

The magnitude of the thermal stress state is proportionate to both substrate temperature and CTE mismatch, which can be seen in the tantalum and aluminum pairing ($\Delta\alpha = -17$) when compared to tantalum on titanium ($\Delta\alpha = -2.5$), where the non-plume quenched thermal stresses are -331.7 MPa and -67.9 MPa, respectively. For samples deposition on titanium substrate, the CTE mismatch for tantalum and nickel coatings were -2.5 and +5.5, respectively, and the smallest of the $\Delta\alpha$ for all four samples. For these samples, the deposition stress is the primary component of residual stress and has a much larger magnitude than the thermal stress.

For all samples, the final residual stress states reduced with the addition of plume quenching. However, the thermal stresses for coatings deposited on titanium show some variability. For tantalum coating on titanium substrate, both the thermal and deposition stresses were increased with the addition of plume quenching, which due to their opposite signs (compressive thermal stress vs. tensile deposition stress) interacted with each other by canceling some magnitude out. The changes in both thermal and deposition stresses for tantalum on titanium were minor and possibly due to processing variability, causing a minimal change in the final stress state.

For nickel coating on titanium substrate, the non-plume quenched and 100 slpm plume quenching flow rate show a decrease with the addition of the plume quenching. However, the 50 slpm plume quenching condition displayed some anomalous behavior as deposition stress heightened and thermal stress dipped below the 100 slpm quenching condition, which would be expected to fall somewhere in between the non-plume quenched and 100 slpm position. The overall residual stress state decreases in an expected trend between all three conditions, although the 50 slpm condition decreases because of unexpectedly low thermal stress in combination with unexpectedly high deposition stress. However, the evolving stress (stress generated layer by layer) for the three plume quenching conditions showed little difference and similar stress generation during deposition.

Although some irregularity is seen for substrate-coating pairings with deposition stress being the primary residual stress component, there is a consistent pattern of plume quenching reducing thermal (and resulting residual stress) for pairings with large CTE mismatch and dominating thermal stress components.

5.6 Sample Variability in Typical Processing vs. Plume Quenching

For many of the experimental results, the compared results between plume quenching conditions showed less variation when compared to the variability created by the sample fixturing, position, and separate runs. As a cooling tool or processing technique, having less variability than typical processing components (sample geometries, fixturing during spray, runs on different days with different weather or ambient conditions) shows how little of an effect plume quenching has on characteristics such as coating deposition efficiency, porosity, and modulus.

Chapter 6

Conclusions

Plume quenching is a cooling technique that targets the plume itself with the intention of redirecting the hot plume gases before they can interact with the substrate, reducing the substrate temperature by preventing heat absorption. Substrate temperature control is necessary in temperature sensitive workpieces, as well as for controlling residual stresses, and allows for increased time on the part (allowing for faster deposition without any cooling downtime). Plume quenching at 50 and 100 slpm has been shown to reduce substrate temperatures, with the cooling effect increasing with the plume quench flow rate. To prove the viability of plume quenching as a cooling technique, critical coating characteristics such as deposition efficiency, density, microstructure, modulus, and adhesion strength were examined. Plume quenching was shown to not interfere with these properties and deemed suitable as a cooling mechanism.

The substrate temperature reduction achieved by plume quenching was shown to reduce the thermal component of residual stress in coatings, which was particularly significant in coatings with large CTE mismatches driving the final stress state, which was seen in the case of tantalum coatings on aluminum substrates. By targeting cooling to the plume rather than the substrate, the plume quenching technique can be agnostic of the workpiece and provide a solution for complex geometries and workpieces that require moderate substrate temperature reduction and residual stress management.

Future Work

While initial results show plume quenching as a promising technique for moderate substrate cooling, flow rates were only tested up to 100 slpm and the extended range of the flow rates have not been probed. There is room for investigation into higher flow rates, which may show a threshold where the plume quenching gas jet begins to influence the coating deposition and properties, as well as various plume quench nozzle geometry (optimizing gas deflection by varying injection velocity and imparted momentum). Additionally, the configuration of the plume quench location relative to the torch face and plume centerline was not varied with this study and could be examined, which if placed closer to the torch face or further may change the ability for particles to heat up or cool them down prematurely.

Future exploration should also take the opportunity to examine nickel plume properties that were not explored due to poor illumination. Adhesion testing could also be expanded to a wider range of materials to investigate lower bond strengths that are below the adhesive strength, which may point to differences caused by the addition of plume quench that were not seen for the titanium substrate adhesion tests. Lastly, the coating and substrate material range can be expanded to look at the effect of plume quenching on other material pairings with large CTE differences or sensitive substrate materials.

Chapter 7

References

[1] Herman H, Sampath S, McCune R. Thermal Spray: Current Status and Future Trends. MRS Bulletin. 2000;25:17-25.

[2] Tucker RC, Jr. Introduction to Thermal Spray Technology. Thermal Spray Technology: ASM International; 2013. p. 0.

[3] DiStefano JR, Pint BA, DeVan JH. Oxidation of refractory metals in air and low pressure oxygen gas. International Journal of Refractory Metals and Hard Materials. 2000;18:237-43.

[4] Vackel A, Mahaffey JT, Fonseca J, Miller AS, Holmes TD, Clearwater M. Controlled Atmosphere Plasma Spray (CAPS) and Cold Spray (CS) for High Purity Metal Deposits. Sandia National Lab.(SNL-NM), Albuquerque, NM (United States); 2019.

[5] Heimann RB. Plasma-spray coating: principles and applications: John Wiley & Sons; 2008.

[6] Kuroda S, Clyne TW. The quenching stress in thermally sprayed coatings. Thin Solid Films. 1991;200:49-66.

[7] Steffens H, Hoehle H, Ertürk E. Investigations on Cooling by Carbon Dioxide During Plasma Spraying.[UNTERSUCHUNGEN ZUM KUEHLEN MIT KOHLENDIOXID BEIM PLASMASPRITZEN.]. Schweissen und Schneiden/Welding and Cutting. 1981;33:159-64.

[8] Kiilakoski J, Trache R, Björklund S, Joshi S, Vuoristo P. Process Parameter Impact on Suspension-HVOF-Sprayed Cr2O3 Coatings. Journal of Thermal Spray Technology. 2019;28:1933-44.

[9] Kramer CM. Plasma-Sprayed Tantalum/Alumina Cermets. Livermore, CA 94550: Sandia National Laboratories; 1977.

[10] Ambardekar V, Sahoo S, Srivastava DK, Majumder SB, Bandyopadhyay PP. Plasma sprayed CuO coatings for gas sensing and catalytic conversion applications. Sensors and Actuators B: Chemical. 2021;331:129404.

[11] Society TS. ASM Thermal Spray Technology White Paper.

[12] Kitahara S, Hasui A. A study of the bonding mechanism of sprayed coatings. Journal of Vacuum Science and Technology. 1974;11:747-53.

[13] Fauchais P. Understanding plasma spraying. Journal of Physics D: Applied Physics. 2004;37:R86.

[14] Surface Coating Systems. DM 3100-PS Plasma Spray2020.

[15] Osborne MC, Abraham. Tantalum and Niobium Powders for Cold Spray Applications. Global Advanced Metals2022.

[16] Brossa F, Piatti G, Bardy M. Tantalum protective coatings for fusion reactor applications. Journal of Nuclear Materials. 1981;103:261-5.

[17] Jr. JAS. Tantalum: The Refractory Metal with Low- and High-Temperature Applications. Journal of Electronic Materials. 1997:25.

[18] Awaludin Z, Okajima T, Ohsaka T. Electroreduced Tantalum Pentaoxide for Hydrogen Evolution Reaction GC GC TaO x , Ta <5+ + e Electrochemical reductive treatment The Chemical Society of Japan Electroreduced Tantalum Pentaoxide for Hydrogen Evolution Reaction. Chemistry Letters. 2014;43:1248-50.

[19] Wang H-T, Li C-J, Yang G-J, Li C-X. Effect of heat treatment on the microstructure and property of cold-sprayed nanostructured FeAl/Al 2O 3 intermetallic composite coating. Vacuum. 2008;83:146-52.

[20] Crawmer DE. Coating Structures, Properties, and Materials. Thermal Spray Technology: ASM International; 2013. p. 0.

[21] Dallaire S. Influence of temperature on the bonding mechanism of plasma-sprayed coatings. Thin Solid Films. 1982;95:237-44.

[22] Pershin V, Lufitha M, Chandra S, Mostaghimi J. Effect of substrate temperature on adhesion strength of plasma-sprayed nickel coatings. Journal of Thermal Spray Technology. 2003;12:370-6.

[23] Boulos MI, Fauchais PL, Heberlein JVR. DC Plasma Spraying, Fundamentals. In: Boulos MI, Fauchais PL, Heberlein JVR, editors. Thermal Spray Fundamentals: From Powder to Part. Cham: Springer International Publishing; 2021. p. 303-59.

[24] Sampath S, Jiang X, Kulkarni A, Matejicek J, Gilmore DL, Neiser RA. Development of process maps for plasma spray: case study for molybdenum. Materials Science and Engineering: A. 2003;348:54-66.

[25] ASTM E3057-16. Standard Test Method for Measuring Heat Flux Using Directional Flame Thermometers with Advanced Data Analysis Technique. West Conshohocken, PA, 19428-2959, USA: ASTM International.

[26] PIDS Technology. Beckman Coulter.

[27] Otsu N. A Threshold Selection Method from Gray-Level Histograms. IEEE Transactions on Systems, Man, and Cybernetics. 1979;9:62-6.

[28] ASTM-C633-13. Standard Test Method for Adhesion or Cohesion Strength of Thermal Spray Coatings. West Conshohocken, PA, 1942802959, USA: ASTM International; 2021.

[29] Landa M, Urbánek P, Kroupa F, Neufuss K. Effect of uniaxial pressure on ultrasound velocities and elastic moduli in plasma-sprayed ceramics. Journal of Thermal Spray Technology. 2003;12:226-33.

[30] Nakamura T, Liu Y. Determination of nonlinear properties of thermal sprayed ceramic coatings via inverse analysis. International Journal of Solids and Structures. 2007;44:1990-2009.

[31] Dwivedi G, Nakamura T, Sampath S. Determination of Thermal Spray Coating Property with Curvature Measurements. Journal of Thermal Spray Technology. 2013;22:1337-47.

[32] Vackel A, Peleg E, Varga J, Blea M, Schmidt C, Gildersleeve E. Elastic measurements of plasma spray refractory metal coatings using thermal cycling of bi-layered beams. ITSC2022: ASM International; 2022. p. 736-42.

[33] Stoney GG. The Tension of Metallic Films Deposited by Electrolysis. Proceedings of The Royal Society A: Mathematical, Physical and Engineering Sciences.82:172-5.

[34] Pfender E, Fincke J, Spores R. Entrainment of cold gas into thermal plasma jets. Plasma Chemistry and Plasma Processing. 1991;11:529-43.

[35] Technology NIoSa. Argon. NIST Chemistry WebBook, SRD 69: National Institute of Standards and Technology; 2021.